PLOS WATER
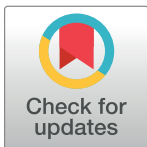
Monitoring Indian ungauged small reservoirs volume from remote sensing: Feasibility, bias and perspectives

Claire Pascal[1], Sylvain Ferrant[1]*, Santiago Peña-Luque[2], Adrien Selles[3,4], Jean-Christophe Marechal[3,4], Taeken Wijmer[1], Simon Gascoin[1], Olivier Merlin[1]

1 CESBIO, Université de Toulouse, CNES/CNRS/INRAE/IRD/UT3, Toulouse, France, 2 CNES, Toulouse, France, 3 BRGM, Université de Montpellier, Montpellier, France, 4 G-Eau, INRAE, CIRAD, IRD, AgroParisTech, Institut Agro, BRGM, Montpellier, France

* sylvain.ferrant@ird.fr

Abstract

What remote sensing products can be used to better quantify the water stored in hundreds of thousands Indian Small Reservoirs (SR)? This ungauged hydrological component of the water cycle is intermittently filled with rainwater runoff, constantly reshaped by farmers since last two decades, crucial for upstream irrigated agriculture. Given the small size and shallow depth of those reservoirs, usual remote sensing techniques (Altimeters and LIDAR) used in spatial hydrology to monitor their water level are not adapted. We evaluated the uncertainty of SR volume retrieval methods based on surface water estimates from Sentinel-2 and associated volumes from global available DEM at a medium to coarse resolution. Four pair of stereoscopic images at Very High Resolution (VHR) from Pléiades satellites were acquired during the last two dry hydrological years (2016 and 2019), when SR were totally empty. The Pléiades DEMs produced were cross validated with LIDAR IceSAT-2 products, and used to extract 504 SR bathymetries within an area covering 1,813 km^2 located in the Telangana state (114,789 km^2). We compared Pléiades based retrievals to freely available regional to global DEM to explore the regional volume retrieval Bias: ALOS World 3D-30 m, WorldDEM GLO-30 at 30 m TanDEM-X DEM at 90 m and one Indian DEM (CartoDEM at 30 m). The Mean Absolute Percentage Error (MAPE) of reservoir volumes from global DEMs range from 47% to 78%. MAPE are 17%, 29% and 46% for Pléiades DEM resampled at 12, 30 and 90 m, respectively. In a near future, upcoming stereoscopy satellite missions at lower costs and with larger coverage and shorter revisit such as CO3D will provide 12m or higher resolution DEMs that, if acquired in dry years, will lead to acceptable MAPE (< 20%), to monitor empty SR geometries throughout India and other semi-arid areas in the world.

1 Introduction

Many semi-arid regions were foreseen to and are nowadays facing increasing water stressors, both linked to irrigation water and domestic demand increase, to sustain food production and

urban area growth [1]. Among those regions, India, the nation with the largest population, is the "world most water-stressed country" according to the World Bank. To cope with these increasing stressors, many hydrological infrastructures were, are and will be built to manage surface and groundwater availability: big dams and canals to store stream water along rivers for irrigation command area and electrical power production; Small Reservoirs (SR) to catch runoff upstream; more recently mega-basins to store pumped water for irrigation and domestic water (Kaleshwaram project). Contrary to big surface reservoirs, resulting from river dam installations, small reservoirs (SR), or tanks, are less inventoried and not monitored. Yet, they are known to have a strong impact on hydrology [2]. Increasing the number of SR, especially in upstream regions, is a common adaptation to water stress [3, 4]. In South India, SR are used to catch monsoon rainfall runoff in upstream areas, to sustain crop irrigation and maintain open water for cattle during the following dry season. SR have also been promoted to enhance aquifer recharge [5], which has been questioned in terms of efficiency as the loss associated with direct evaporation could be high [6–8].

This Indian traditional Rainwater Harvesting System (RHS) is composed of hundreds of thousands of SR, spread along a non perennial drainage network. In the Telangana State, a typical SR consists in a flat depression of around one kilometer wide, dammed with an earthen dike of 3 to 10 meters high and about 20 meters wide, that often completely dries up during the dry season. In this Indian state, a costly 5-year program named Mission Kakatiya started in 2015 to rejuvenate more than 46,000 SR, i.e. excavating for a few meters to desilt the bottom part and thus enhance the aquifer recharge and create new ones. A similar water body rejuvenation scheme called Mission Amrit Sarovar has been launched in 2022 (https://rural.nic.in/en/press-release/mission-amrit-sarovar). These programs show the socio-political importance of the RHS related to food security, but also its fast structural changes following a growing water demand.

Quantifying the storage capacity and monitoring the seasonal fluctuations of the volume stored in this RHS is hence crucial to estimate water stocks and forecast spatial stressors in upstream areas, disconnected from main surface water resources (large dams and rivers). This hydrological network is too scattered to be monitored with altimeters such as Envisat, ICE-SAT, Topex/Poseidon measurements [9–12], or the more recent altimeter onboard on Sentinel-3, used on West African lakes [13]. We used Icesat-2 to illustrate this limitation. The volume retrieval is challenging due to the large number and small size, together with a lack of in-situ monitoring systems. However, current space-borne missions and products open new possibilities. Surface water fluctuation retrieval from either radar or optical data are available. Landsat data covering 40 years have been processed to produce monthly water maps [14, 15]. Recent studies have explored the capacities and accuracies of Sentinel missions to retrieve regional surface water dynamics [16, 17] with a focus on radar and optical related bias to this retrieval [18].

The multiplication of satellite missions for Earth topography mapping led to the release of free access global Digital Elevation Model (DEM) such as Advanced Space-borne Thermal Emission and Reflection Radiometer (ASTER) [19], TanDEM-X DEM [20], Advanced Land Observing Satellite "DAICHI" (ALOS) World 3D-30m [21] and Copernicus's WorldDEM GLO-30, with a resolution up to 30 m. This encouraged the development of methods for surface water volume retrieval using the bathymetry derived from DEM combined with either altimeter data [22], satellite Lidar transects [23] or time series of surface water extent derived from Landsat [22, 24, 25] or Sentinel-1 specifically used for high cloud cover context [26].

In most cases, the acquisition date of the DEMs cannot be chosen by the user which results in impossible retrieval of the bottom geometry of reservoirs due to the presence of vegetation or water. To cope with these imperfections, the reservoir geometry is often simplified with a

pre-definite trapezoidal shape [9, 22, 27], by topographic continuity along channels [28] or by modeling the volume-area relationship [9, 24–26].

Several approaches of volume estimates methods at regional scale have been tested for large reservoirs [11, 22, 25] and more recently for SR [26, 29]. In particular, a previous study has reported the interest of high resolution remote sensing data to retrieve the volume-area relationships for SR of the RHS in South India, Tamil Nadu state, using the TanDEM-X DEM commercial product at 12-m resolution [26]. This study has estimated a fluctuation of 8.2 million cubic meter (MCM) of surface water in 559 SR over a region of 5,647 km^2 using dynamic surface water mapping. According to the authors, the limitations of this study are (i) the surface water area detection accuracy based on Sentinel-1 radar data and (ii) the simplification of reservoirs' geometry with power volume-area relationships due to the low DEM precision.

However, to this date, the freely available global DEMs have a resolution coarser than that of TanDEM-X DEM commercial product. For instance, it is 30 m for ALOS World 3D-30m, WorldDEM GLO-30 and CartoDEM or 90 m for TanDEM-X non-commercial DEM.

Recent high-resolution on-demand DEMs like the ones produced from Pléiades very-high (70 cm) resolution (VHR) stereoscopic images allow controlling the acquisition date and therefore allow the accurate retrieval of reservoir bathymetry. A previous study estimated the total capacity of whole SR of the RHS of the Telangana State to about 30 mm (3.4 km^3) using Global Surface Water database [14], Pléiades DEM and Sentinel-2-derived Maximum Water Area Extent (MWAE) [30]. Here, we will compare the surface-volume relationship derived from this high resolution DEM with other available global DEM. Yet they are commercial products only available locally, as Pléiades scenes typically only cover a 20×20 km^2 area [31]. On the other hand, upcoming very high resolution stereoscopy satellite missions such as CO3D [32] will provide VHR DEM cheaper than Pléiades with a high temporal frequency. These DEMs will be crucial to monitor a high number of these SR, as it has been done only for individual SR so far [6–8]. In addition, regional studies on SR have not been attempted with freely available DEMs because of their coarse ($\geq$30m) resolution, although there has been two attempts with a commercial 12-m DEM [26, 29]. The objective of this study is to quantify the efficiency of VHR DEM acquired during dry periods (such as Pléiades or those from CO3D available in the near future), compared to currently available global coarse DEM, for the retrieval of surface water volumes of SR composing the Indian RHS.

We produced VHR DEM from Pléiades stereoscopy, acquired during dry years while SR are empty. We evaluated the accuracy of the geometry retrieval with available IceSAT-2 space borne Lidar elevation transects. We were able to extract 505 SR bathymetries over an area covering 1,813 km^2 in the Telangana state. Hypsometry (i.e. volume as a function of the surface) relationship are derived from each SR at 2m resolution and are considered as a reference, i.e. not a ground truth but the most realistic bathymetry with both the best spatial resolution and an total absence of water. We explored the drifts in volume estimates induced by coarser resolution DEMs: 1- upscaled by resampling Pléiades DEM or 2- extracted from global to national available DEMs CartoDEM (30-m Indian DEM), Copernicus WorldDEM GLO-30, ALOS World 3D-30 m (30-m global DEMs) and TanDEM-X DEM (90-m global DEM).

2 Materials and methods

2.1 Study area

The Telangana State (114,789 km^2) is a highly irrigated region in South India with a high population density (about 335 inhabitants per km^2 in 2020 according to the Unique Identification Authority of India (UIDAI)), dominated by a semi-arid climate. The monsoon precipitation occurs between July and October and ranges from 540 to 1,300 mm with a mean of 879 mm
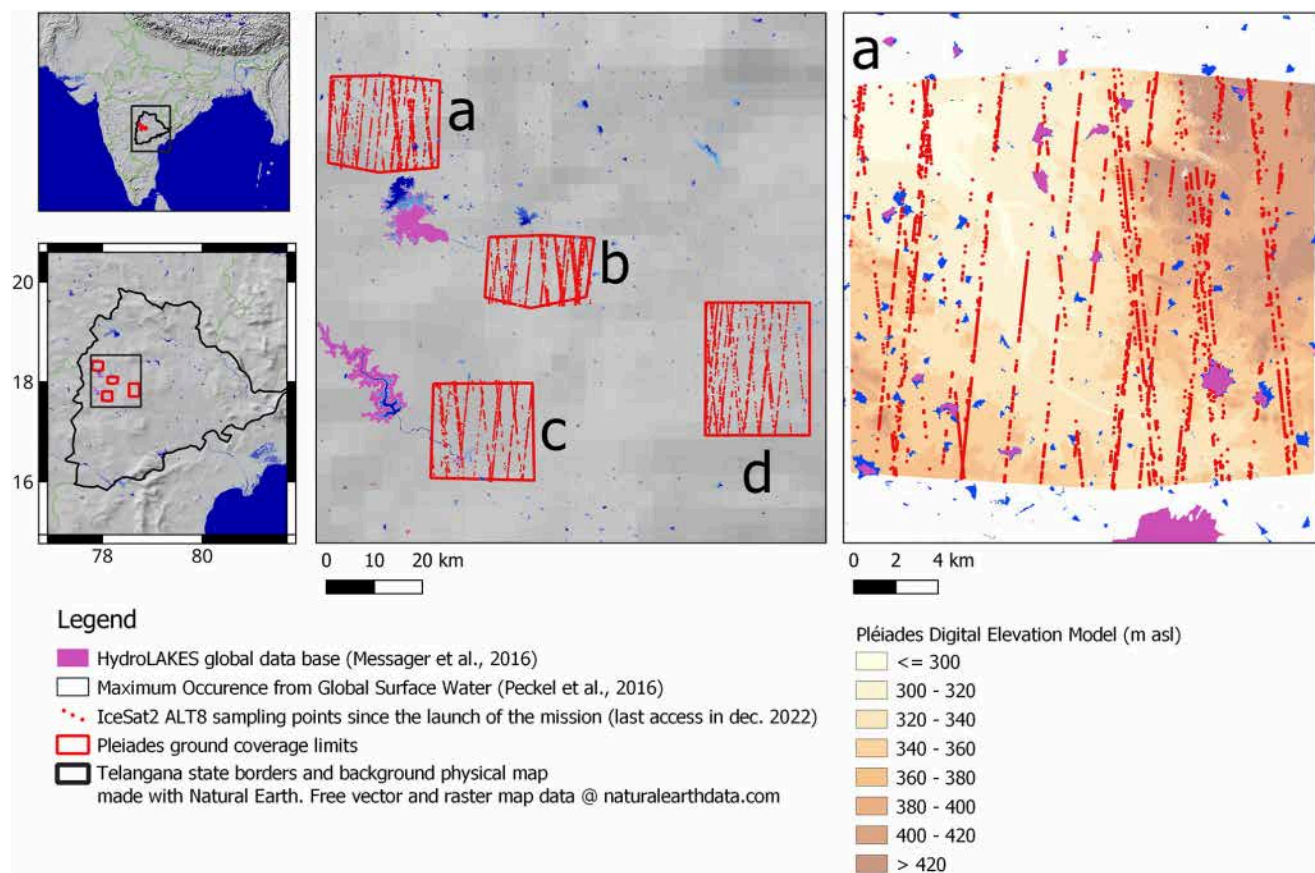
Fig 1. Location of the study area. The four Pléiades scenes (a), (b), (c) and (d) (green rectangles) are located in the western part of the Telangana State. The 25 main dam lakes identified in the GRanD inventory (Lehner et al., 2011) are represented in magenta. The image on the right shows a zoom on the DEM on scene (d) with Pléiades elevations in gradient of browns. The location of the small reservoirs (SR) of the Rainwater Harvesting System (RHS) is indicated by the Global Surface Water database in blue, and the location of the whole IceSAT-2 ATL08 dataset are illustrated with red dots along IceSAT-2 tracks. The background and state border can be downloaded here: http://www.naturalearthdata.com.

https://doi.org/10.1371/journal.pwat.0000260.g001

(Indian Meteorological Department). In this area, groundwater is complementing the surface water resource to sustain one or two growing seasons of irrigated crops in a year. The irrigated water demand strongly varies with the available water resource, from 51 to 310 mm per growing season in upstream areas [33, 34].

The majority of the State (57%) is composed of a shallow fractured granitic aquifer characterized by high fluctuations due to water pumping [35]. Monsoon rainfall is stored on the surface by large dam reservoirs built along rivers. The Indian National Register of Large Dams (NRLD) reports 126 dam lakes with a cumulative capacity of 113 mm. The 25 largest reservoirs, referenced in the global GRanD inventory [36], are shown in magenta in Fig 1. In upstream areas, surface water is available only in the RHS ($<$ 3% of the area), a network of non-perennial SR filled during the monsoon season, drained quickly during the dry season. These structures are also promoted for aquifer recharge enhancement [7].

2.2 DEM

In the following, we present the characteristics of available global DEMs that we have selected to explore the possibility to estimate volumes stored in the Telangana ungauged RHS. The

Table 1. DEM used, their resolution, sensors and acquisition date.

DEM	Horizontal resolution	Data type	Acquisition date	Sensor (resolution)
Pléiades (Airbus)	2 m	float	(a): 01-06-2016; (b): 14-06-2016; (c): 16-06-2016; (d): 16-06-2019	Pléiades optical stereoscopy (50 cm)
CartoDEM (ISRO)	30 m	integer	2006-2016 (Composite DEM from multiple acquisitions)	Stereo panchromatic images Cartosat-1 (2.5 m)
TanDEM-X DEM (EOC)	90 m	float	2010-2015 (Composite DEM from multiple acquisitions)	X-Band interferometric SAR TanDEM-X (2.4 m—4 m)
WorldDEM GLO-30 (Copernicus)	30 m	float	2010-2015 (Composite DEM from multiple acquisitions)	X-Band interferometric SAR TanDEM-X (2.4 m—4 m)
ALOS World 3D-30m (JAXA)	30 m	integer	2006-2011 (Composite DEM from multiple acquisitions)	Composite DEM from multiple acquisitions PRISM panchromatic optical sensor ALOS (2.5 m)

https://doi.org/10.1371/journal.pwat.0000260.t001

main information on the DEMs used in this study are summarized in Table 1. Each DEM have a surface water mask corresponding to the surface water at the period of acquisition, except for the four Pléiades DEM that were acquired during dry periods. The main information on the DEMs used in this study are summarized in Table 1. The filling ratio—the ratio of surface water at the moment of DEM based satellite acquisition with the maximum surface water (MWAE)—are presented in Table 3 for each global DEM.

2.2.1 Pléiades 2-m DEM. The Pléiades stereoscopic images used in this study include 3 stereo-pairs that were acquired in June 2016 (available in Airbus Defense and Space catalogue before this study, images (a), (b), (c) in Fig 1) and one stereo-pair acquired in June 2019 (specifically tasked for the purpose of this study, image (d) in Fig 1), and cover respectively 444, 322, 463 and 584 km^2. The images (available online, 10.5281/zenodo.10403040) were selected or acquired at the end of the dry season, while SR were empty. In those four areas, a 2-m resolution DEM was generated using the panchromatic stereoscopic images and the NASA Ames Stereo Pipeline (ASP) software V2.6.2 [37]. The photogrammetric process was done using the rational polynomial coefficient provided by the satellite operator. First, we generated point cloud from the panchromatic images with the block matching algorithm of the stereo utility of ASP [38]. Then, we rasterized the point cloud on a 2-m resolution UTM grid using the point2-dem tool of ASP [39]. In the 3 archives scenes, some areas covered by water (river bed essentially) or bright soils for which the reflectances were saturated have no valid elevation values, explaining No-Data values. In the acquisition of June 2019, cloud presence also led to no data values in the DEM.

2.2.2 IceSAT-2 ATL08 and ATL03 elevation transects. We downloaded the whole archive—intersecting the four study sites—of the Advanced Topographic Laser Altimeter System (ATLAS) instrument on board the Ice, Cloud and land Elevation Satellite-2 (IceSAT-2) observatory (since 2018). IceSAT-2 ATL08 product [40] is built per granule (100m along track elevation estimates) based on the ATL03 product [41] containing geolocated ellipsoidal heights for each time tagged photon event corrected for several geophysical phenomena (e.g. atmospheric refraction, tides). We used ATL08 data to assess the Pléiades DEM accucracy over the whole study area (Fig 1 and Table 2). Uncertainties of the elevation estimates (provided by NASA) are high in this area, as presented in Table 2. ATL03 product—Geolocated ellipsoidal heights for each time tagged photon event, is useful to compare Pléiades DEM on the bund/dam geometries, not caught at 100m with ATL08. It is used to build Figs 4 and 5. ATL03 product—Geolocated ellipsoidal heights for each time tagged photon event. ATL03 provides a denser point cloud than ATM08. It is useful to characterize the bund/dam geometry when Ice-SAT-2 track cross one of them (used to build Figs 4 and 5). However it contains more noise

Table 2. IceSAT-2 ATL08 versus Pléiades elevation Bias, STD, NMAD and average uncertainties in meters for each IceSAT-2 ground tracks found since 2018 over Pléiades scenes. IceSAT-2 elevation uncertainty < 4 meters are excluded.

Pléiades Scene	Bias	STD	NMAD	Selection ratio *	ATL08 Average uncertainty
Scene a	3.5	0.8	0.6	595 / 2374	2.5
Scene b	4.4	1.0	0.5	888 / 2763	2.6
Scene c	4.6	3.8	0.6	408 / 1829	2.7
Scene d	2.8	0.8	0.5	465 / 2437	2.8

* IceSAT-2 elevation uncertainty < 4 meters are excluded.

https://doi.org/10.1371/journal.pwat.0000260.t002

due to atmospheric and vegetation scattering and needs to be filtered to retrieve a ground elevation profile. The filtering method used for ATL03 is described in section 3.1.2 and the results are shown in Figs 4 and 5. Both are used to quantitatively and qualitatively discuss the accuracy of Pleiades DEM for this hydrological application. The main difficulty we encountered is that the spatial LIDAR data are highly affected by Indian atmospheric optical thickness that alters photon time travel. The dispersion of the photon cloud is high in Fig 4, and very small in Fig 5, a clear sky day. In addition, we selected some ATL03 tracks to investigate the accuracy of topographic profiles derived from Pléiades accross a few SR.

2.2.3 CartoDEM. The Cartosat-1 Digital Elevation Model (CartoDEM) is provided by the Indian Space Research Organization (ISRO). It is produced from stereo panchromatic images from Cartosat-1 at a 2.5-m resolution and the water surfaces were flattened. It is provided with a horizontal resolution of 30 m and elevation values are rounded to the meter. The accuracy of CartoDEM was estimated on three test areas against control points, with a RMSE ranging from 3.4 to 4.72 m and a linear error at a 90% confidence level ranging from 4.7 and 7.3 m [42].

2.2.4 TanDEM-X DEM. TanDEM-X DEM is a global DEM generated from bistatic X-Band interferometric SAR acquisitions of TerraSAR-X and TanDEM-X satellites. The TanDEM-X mission was financed by a Public-Private Partnership between DLR (German Aerospace Centre) and Airbus Defence & Space. The DEM is produced with acquisitions ranging from December 12, 2010 to January 16, 2015. It has a native resolution of 0.4 arcseconds (<10 m) and is provided with a horizontal resolution of 3 arcseconds (90 m) and a vertical accuracy <2 m for slopes <20%, and <4 m for slopes <40% [43]. Water body heights are not edited in the DEM.

2.2.5 Copernicus WorldDEM GLO-30. The Copernicus DEM is a Digital Surface Model (DSM) produced with the data from the TanDEM-X mission. The instance used for this study is GLO-30, a global DEM with a resolution of 30 m and the same vertical accuracy as TanDEM-X DEM. Water bodies are flattened and consistent flow of rivers are included.

2.2.6 ALOS World 3D-30m. ALOS World 3D-30m (AW3D30) Version 3.2. is a global DSM processed by the Japan Aerospace Exploration Agency (JAXA). It is produced from stereoscopic panchromatic optical images from the Panchromatic Remote-sensing Instrument for Stereo Mapping (PRISM) sensor of the Advanced Land Observing Satellite "DAICHI" (ALOS) which operated from 2006 to 2011. It is provided with a spatial resolution of 30 m and elevation values are rounded to the meter. The accuracy of AW3D30 is expressed as a RMSE of 5 m in both vertical and horizontal directions [44]. Water bodies are not edited.

2.2.7 Pléiades at coarser resolution. The 2-m Pléiades DEMs were aggregated at 12 m (resolution of TanDEM-X DEM commercial product), 30 m and 90 m using bilinear resampling. This interpolation method is the most robust and appropriate for DEM, rather than nearest neighbor or cubic. This allows us to isolate the effect of DEM resolution on SR geometries.

2.3 Sentinel-2 images

Sentinel-2 is a constellation of two satellites launched in June 2015 and March 2017 that deliver multispectral images at 10- and 20-m resolution and a revisit time of five days. We used Sentinel-2 multispectral images to track the surface water area evolution in the SR, taking advantage of its 5-day revisit time. We used Sentinel-2 images processed by the MAJA processing chain [45] which detects clouds, cloud shadows and topographic shadows, and corrects reflectance levels from atmospheric phenomena (absorption by atmospheric gases and scattering by air molecules and aerosols). These S2-L2A images were downloaded from Theia data platform (https://www.theia-land.fr/, accessed on August 5th, 2021). A total of 42, 33, 76 and 76 cloud-free Sentinel-2 images over a period of 2 years close to the Pléiades acquisition date were downloaded for scenes (a), (b), (c) and (d) respectively. A random forest classification was used for each S2 acquisition to map surface water area extent in SR. Learning samples were automatically extracted from auxiliary data: HAND((Height above nearest drainage) [46] derived from MERIT DEM [47] for selecting pixel never flooded. Water pixels were extracted from permanent water pixels as observed with Landsat in the Global Surface Water data base [14]. This method is fully described in [18].

3 Methodology

In the following, we describe the method presented in the flowchart of Fig 2.

3.1 Step 1: DEM preprocessing

3.1.1 Preprocessing.   CartoDEM, TanDEM-X DEM, GLO-30 and AW3D30 products are provided with water masks, indicating the presence of water at the time of their acquisition. We used them to mask invalid DEM elevations over surface water, replacing by the theoretical water elevation [29]. All DEMs were then resampled at 2 m with bilinear interpolation for (i) comparable results with Pléiades 2-m DEM and (ii) enough raster values within SR extents to sample their geometries. A bilinear interpolation is also used to aggregate Pléiades DEMS at 12, 30 and 90 meters.

3.1.2 Validation of Pléiades DEM.   We used ATL08 ground elevation product to statistically quantify the differences between Pléiades and IceSAT-2 elevations. This product is an analysis of the raw Lidar measurements corresponding to a ground elevation estimate for a 100m along track with a canopy height. Both elevations are provided with an uncertainty expressed in meters. In this area, this uncertainty is high, probably because of the regular presence of aerosols. We limited this ground elevation uncertainty to less than 4 meters, this limitation corresponding to a fourth of the number of available ATL08 segments. Comparison results are shown in Table 2 in term of Bias, STD and Normalized Median Absolute Deviation (NMAD, Eq 1). This last estimator is particularly adapted for accuracy assessment of Digital Elevation Models [48].

$$NMAD = 1.4826 \cdot median_j(|\Delta h_j - m_{\Delta h}|) \tag{1}$$

To make a more detailed evaluation at fine scale, we selected three ATL03 tracks that cross a SR found on each scene a, b and d, to illustrate the differences at higher spatial resolution between Pléiades, ATL03 and ALOS DEM on the along-track IceSAT-2 acquisition. Several methods are used to detect outliers in altimetric data methods [49]. Most of them rely on detecting the anomalies of data points regarding their spatial environment. In our study, we relied on a custom method estimating the most likely altitude in the local
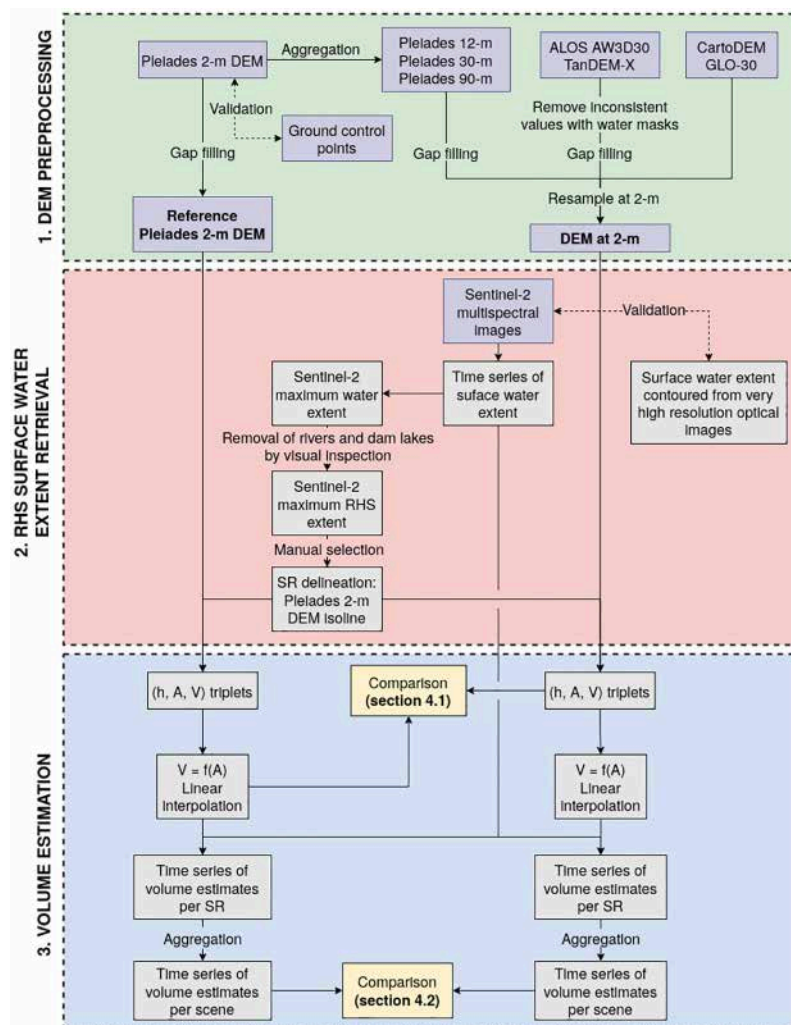
Fig 2. Schematic flow diagram of the proposed method for volume estimation. SR: small reservoir. RHS: Rainwater Harvesting System. h, A, V: height, area and volume. V = f(A): volume-area relationship.

https://doi.org/10.1371/journal.pwat.0000260.g002

environment of the measurement and used a threshold to allow for plausible local high-frequency variations.

In practice, we discretized the altitudes in intervals of 30 cm, to identify the height window containing the most observations. This operation is applied using a moving window of N consecutive acquisitions. This operation results in a series of height windows for which the mean value corresponding to the original data points is recorded. The dataset is then filtered to keep only altitudes with a deviation of less than 50cm from those mean values. This method was used instead of a moving average technique as, in this particular dataset, we expect skewed error distributions and high levels of noise. This skewness and noise are mainly due to the presence of aerosols in the area which leads to a large number of strong overestimation of surface altitude in the datasets. Nonetheless, it is important to stress that this method is sensitive to the discretization interval, the number of consecutive pixels used to build the distributions and the tolerance thresholds that were manually fine-tuned in this study. The elevation profiles comparison is shown in Figs 4 and 5.

3.2 Step 2: RHS surface water extent retrieval from Sentinel-2 data

3.2.1 Time series of surface water area extents. Surface water maps were produced from the time series of Sentinel-2 images at 10-m resolution. The surface water maps were obtained from a supervised classification at pixel level using the random forest algorithm [50], commonly used in surface water detection [51, 52]. A training data set was selected for each Sentinel-2 L2A product using a randomized selection of 10,000 pixels, including 2,000 water samples. The water pixels were selected from permanent water identified from the Global Surface Water occurrence dataset [14] and the HAND (Height Above Nearest Drainage) data-set [46] was used to select non water pixels. We built the model on 100 trees and used Sentinel-2 bands B3, B4, B8, B11, B12, as well as the NDWI [53] and MNDWI [54] indices for classification. This method is known to be robust and showed a good accuracy in temperate areas [18].

3.2.2 Validation of surface water maps. The accuracy of Sentinel-2-derived water maps was evaluated against very high resolution historical images from Google Earth Pro (Maxar Technologies or CNES/Airbus images) between 2016 and 2020. We manually contoured water extents for 16 SR at several time steps that matched Sentinel-2 acquisition date up to to five days, for a total of 29 pairs of SR and dates.

3.2.3 SR Maximal Water Area Extent (MWAE) delineation and maximum water height. The maximal water area extension is almost never observed as it is rarely reached. Furthermore, the presence of vegetation within this rarely flooded areas decrease the capacity of optical or radar data to detect accurately their exact contours. We have first extracted Landsat derived MWAE from the Global Surface Water repository at the Telangana scale (available online, 10.5281/zenodo.10402096) and from Sentinel-2 water mask time series produced only over the Pléiades scenes, by superimposing and merging them (available online, 10.5281/zenodo.10402199). These contours were refined by removing (i) the areas corresponding to river bed and dammed river reservoirs, (ii) SR containing more than 5% of Pléiades 2-m DEM no-data and (iii) areas inferior than 1,000 m^2, threshold below which they are considered temporary puddles and not dug structures. This led to the identification of 505 SR over the 4 Pléiades scenes, composing the RHS: 112 on scene (a), 91 on (b), 114 on (c) and 188 on (d). Their size varies from 1,000 m^2 to 185 ha, and they cumulatively represent 4,100 ha over the 1,813 km^2 study area.

We have then built manually a theoretical MWAE by selecting, for each 504 SR, the most appropriate elevation isoline in the Pléiades DEM, using this satellite derived MWAE contour shape (available online, 10.5281/zenodo.10402355). This selection by hand, based on our field expertise enable to account for Sentinel-2 or Landsat surface water contour erosion. The selected isoline corresponds to a realistic maximal altitude of the surface water, i.e. the maximum elevation from the bottom of the depression, h_{max} retrieved during this step for each SR (step illustrated in Fig 3).

3.3 Step 3: Volume estimation methods

3.3.1 DEM-based volume estimation method. For each SR delimited by an isoline from Pléiades DEM, paired volume and area estimates were extracted from each DEM at 10 cm height increment, from 0 to the maximum water level reached within the polygon (the height of the isoline h_{max}). For a given water height h, we compute the volume with the true bathymetry by integrating water volumes pixel-wise, as in [26, 29] (Eq (2)).

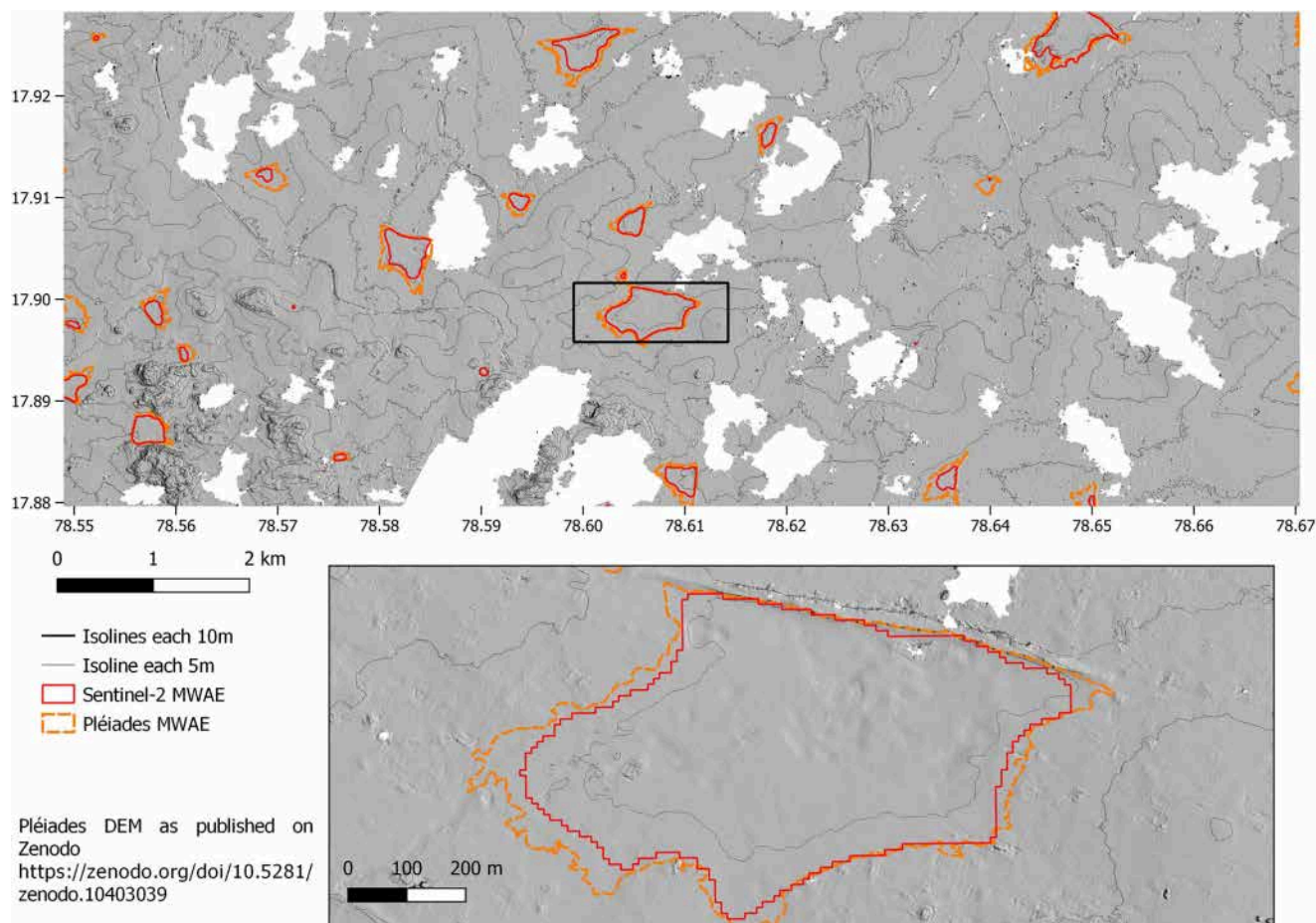$$V_h = A_{pix} \sum_{pix \in A_h} (z_{min} + h - z_{pix})$$

(2)

Fig 3. Comparison of Sentinel-2 multispectral data derived MWAE (red line) and Pléiades very high resolution DEM derived MWAE (orange lines). Orange lines are the elevation lines manually selected for the construction of the hypsometry (Volume as a function of surface) relationship of the 505 small reservoirs of the study. The background is the Pléiades DEM raster viewed as a hillshade (made with QGIS software, data available 10.5281/zenodo. 10403040). White areas corresponds to NoData elevation value due to clouds in the scene d at the time of Pléiades acquisition, 16/06/2019.

https://doi.org/10.1371/journal.pwat.0000260.g003

with h the water level ranging from 0 to h_{max}, A_h the cumulative area of all the pixels within the SR maximum extent and with an elevation below h, A_{pix} the surface of one pixel (4 m^2), h_{max} the water level at maximum capacity. ($z_{min} + h - z_{pix}$) is the water depth for a given pixel, with z_{pix} the altitude of the pixel and z_{min} the lowest altitude of the SR.

3.3.2 SR hypsometric relationships. Hypsometric relationship, i.e. the volume of each SR as a function of surface water are built for each SR using a linear interpolation of each elevation every 10 cm of the VHR DEM pixels inside the Pléiades derived MWAE and below its associated h_{max}. This method allows to take into account the high heterogeneity of the bathymetry retrieved from satellite rather than simplifying it under the form of power [26, 55] or polynomial models [8, 9, 25].

3.3.3 Temporal dynamic of surface water storage at scene scale. Time series Sentinel-2 based water area extents are used to estimate the volume stored at that moment using the hypsometric relationships obtained for each SR. Volumes retrieved from SR were cumulated for each date at scene scale to obtain a regional volume estimate time serie stored in the RHS for each four Pléiades scenes.

3.4 Validation metrics

Three metrics were used to evaluate the fit between the series of predicted values $(\widehat{y_i})_{1 \le i \le N}$ and reference values $(y_i)_{1 \le i \le N}$ for each SR. The coefficient of determination (R^2) is an indicator of the match between observed and predicted values:

$$R^2 = 1 - \frac{\sum_{i=1}^{N} (\widehat{y_i} - y_i)^2}{\sum_{i=1}^{N} (y_i - \bar{y})^2}, \tag{3}$$

where $\bar{y}$ is the average of observed values. The mean absolute percentage error (MAPE) is a measure of the relative error:

$$MAPE = \frac{1}{N} \sum_{i=1}^{N} \frac{|y_i - \widehat{y_i}|}{y_i}, \tag{4}$$

and the mean percentage error (MPE) is a measure of the relative bias:

$$MPE = \frac{1}{N} \sum_{i=1}^{N} \frac{y_i - \widehat{y_i}}{y_i}. \tag{5}$$

A positive MPE (resp. negative) reflects an average underestimation (resp. overestimation) of predicted values against true values. Note that high relative uncertainty for smaller volumes can increase MAPE and MPE despite a low absolute error, and therefore these two metrics must be carefully interpreted. These estimators are the most widely used for forecast accuracies, due to their advantages of scale-independency and interpretability.

4 Results

4.1 IceSAT-2 vs Pléiades comparison

After removing ground elevation with highest uncertainties (> 4 meters), a global estimation of the Bias, standard deviation and Normalized Median Absolute Deviation with Pléiades elevations is presented per Pléiades DEM in Table 2. A scene specific bias varying between 2.8 to 4.6 meters is quantified, with no influence on SR geometries on which we focus in this study. The standard deviations of the residues (differences between both datasets) are similar (around 1m), except for the scene c, which comes from higher elevation discrepancies in this area. It is probably caused by a higher number of Pléiades DEM nodata value in scene c, caused by saturation in reflectance over dry bare-ground in this Pléiades archive taken in June 2016. NMAD is around 0.5m, i.e 50cm, which is acceptable considering the discrepancies between DEM spatial resolution (100 meters vs 2m) and the size of dikes (3 to 10m height).

The Figs 4 and 5 present the location of ATL03 selected tracks for respectively scene a, b and d, with the corresponding Sentinel-2 image at the same acquisition date (left). Elevations along the transects for both Pléiades (red) and IceSAT-2 ATL03 in red and filtered ATL03 (yellow). Elevation Transects are very similar, Pléiades catches better the narrow dike in scene a and the same SR bottom than IceSAT-2 in scene c. ALOS DEM (AW3D), built on ancient ALOS acquisitions (before 2011), is interesting because the RHS was almost empty at that time (Table 3). Whereas the bottom of the SR elevation in scene a (up of the Fig 4) is close to the Pléiades, it is less deep in scene c (down of the Fig 4), explained by the rejuvenation that occurred after 2015: dig of the bottom and increase of the height of the dike that can be seen on aerial images (google earth application). The presence of water at
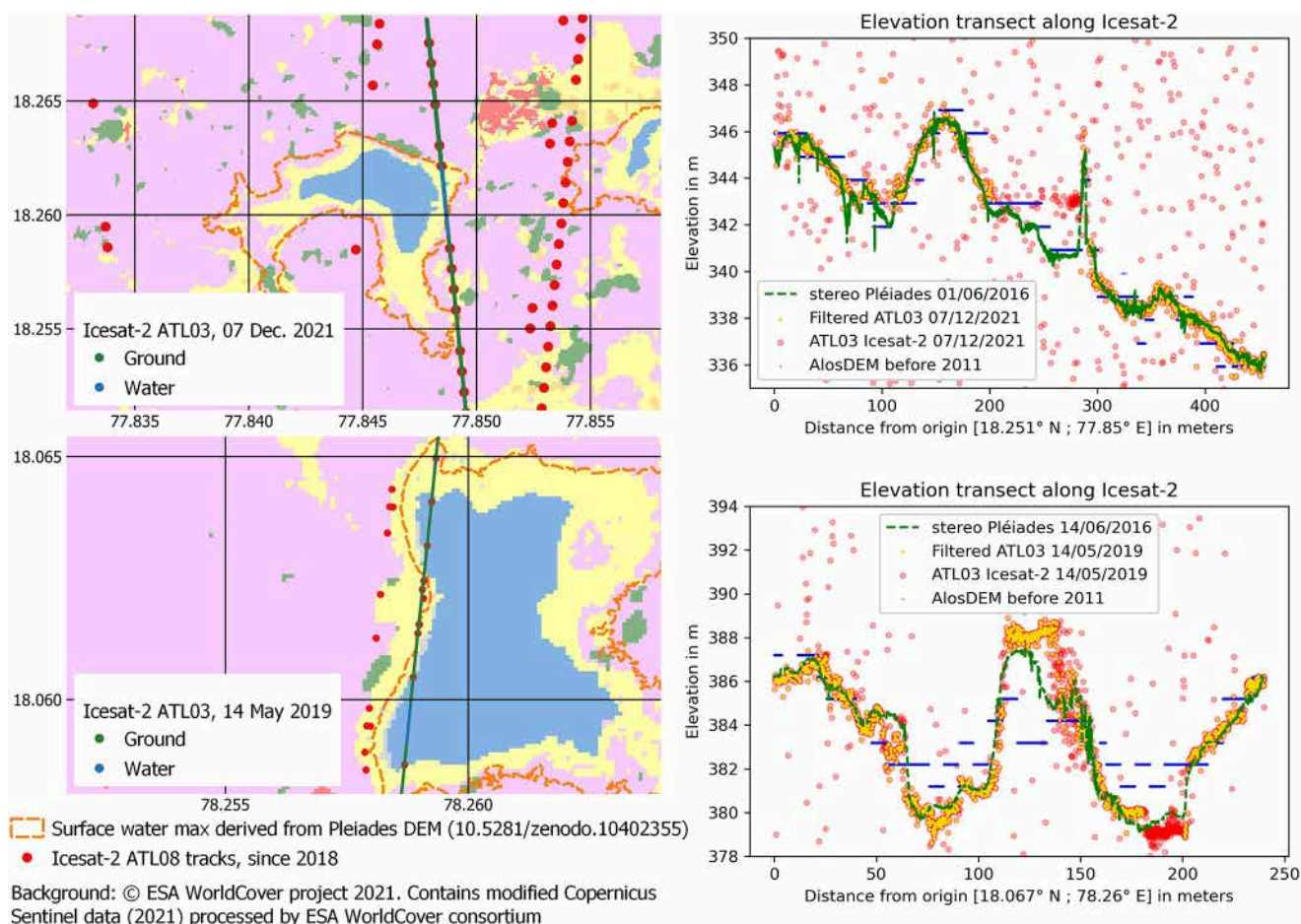
Fig 4. Panel a and b, WorldCover landuse from 2021 is used to represent two Small reservoirs located in Pléiades scene a (up) and b (down). Sentinel-2 images are available for respectively 07/12/2021 and 14/05/2019, the same days of IceSAT-2 acquisition (not shown here for license incompatibilities) and show the presence or absence of water in the small reservoir at the time of IceSAT-2 acquisition. ATL-08 (red dot) and ATL-03 (green dots above ground and blue dots above water at the date of acquisition) are located over the WorldCover background. The maximum water area extent extracted from Pleiades DEM is in orange dashed lines (10.5281/zenodo.10402355). Panel c and d show elevations from Pléiades (dotted green line) along the IceSAT-2 ATL-03 transect represented with green dots in panel a and b, together with ATL03 geolocated photon elevations (red points), maximum likelihood filtered ATL03 ground elevations (Yellow) and AW3D30 DEM elevations in blue dots. Sentinel-2 data were obtained from https://www.copernicus.eu/en/access-data but not used in the published figure.

https://doi.org/10.1371/journal.pwat.0000260.g004

the time of IceSAT-2 acquisition in scene a is clearly visible on the ATL03 data, preventing IceSAT-2 to catch the bathymetry of the SR at this time. The Fig 5 is another example in the scene d of the differences of DEM data over SR. Pléiades and IceSAT-2 elevation are very similar, the dike and SR bottom have the same geometry as both data were obtained from the same period when the SR was empty, whereas it is a bit different from ALOS, empty as well but corresponding to the previous decade. These illustrations are important to understand the importance of DEM spatial resolution, hydrological filling rate and time of acquisition. It also provides a qualitative evalution of the strong ability of Pléiades to retrieve SR geometries.

In the next sections, we consider Pléiades DEM at 2m as a reference to quantify the relative volume errors induced by coarser DEM resolutions and using global DEM for the RHS of this Indian region.
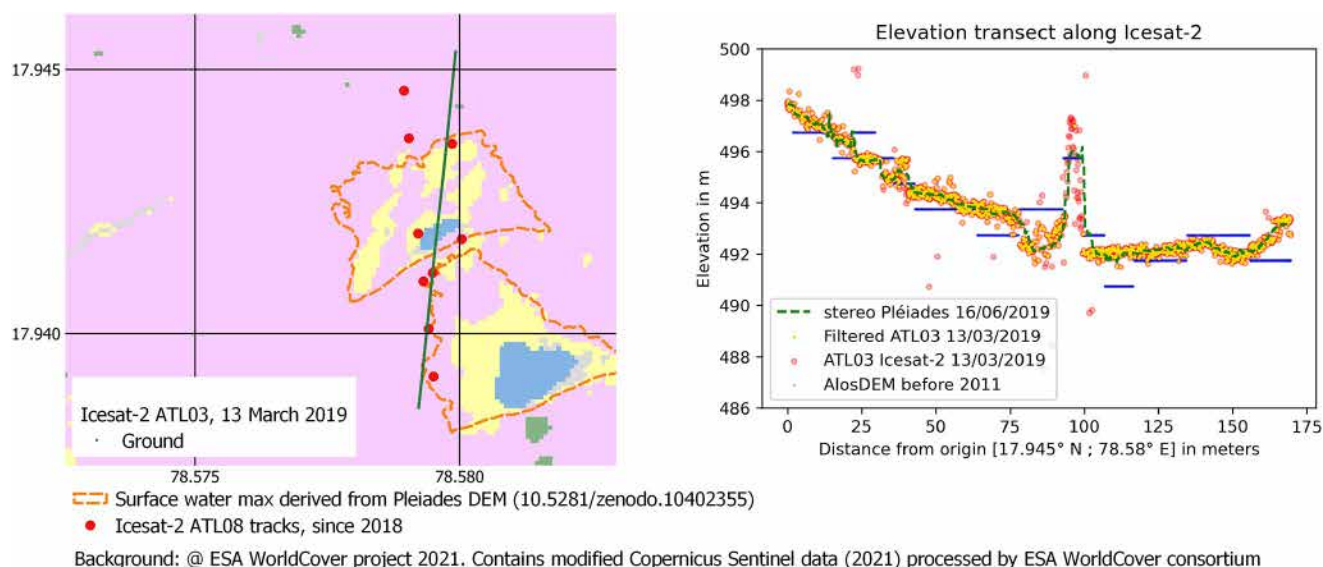
Fig 5. Panel left, WorldCover landuse from 2021 is used to represent the Small reservoir, delineated by its maximum surface water area extent extracted from Pleiades DEM is in orange dashed lines (10.5281/zenodo.10402355). ATL-08 (red dot) and ATL-03 (green dots above ground and blue dots above water at the date of acquisition) are located over the WorldCover background. Panel right, elevations from Pléiades (dotted green line) along the IceSAT-2 ATL-03 transect geolocated photon elevations (red points), maximum likelihood filtered ATL03 ground elevations (Yellow) and AW3D30 DEM elevations in blue dots.

https://doi.org/10.1371/journal.pwat.0000260.g005

4.2 Comparison of SR hypsometry relationships from selected available DEMs

We used the bathymetry from Pléiades 2-m DEM to estimate the potential capacity of the RHS: it is estimated at 57.6 million cubic meters (32 mm) over the 1,813 km^2 study area. The majority of the RHS is composed of SR with a MWAE lower than 5 ha (as shown in the distribution in Fig 6), yet these very small reservoirs represent only between 4 to 11% of the total volume of the RHS on individual Pléiades scenes, and 7% on all four Pléiades scenes (as illustrated in Fig 6b).

Apart from the DEM acquisition timing, i.e. the presence or absence of water—anterior to creation or rejuvenation—each source of DEM acquisition have diverse capacity to retrieve the SR geometries. Fig 7 illustrates those differences for two SR that were empty during the acquisition of all DEMs. Coarse resolution smooths the dike height and the bottom bathymetry (particularly small depressions at the bottom of SR). This leads to systematic volume underestimation. The dike of larger reservoirs (as the 114 ha reservoir in Fig 7a) is well detected by Pléiades at 2- and 12-m. The degradation of Pléiades to a 30-m resolution decrease the dike height by 2, which is globally the same height visible by GLO-30, AW3D30 and CartoDEM. At

Table 3. Filling ratio (%) of the observed Rainwater Harvesting System (RHS) at the acquisition date(s) for CartoDEM, AW3D30, GLO-30 and TanDEM-X DEM. It is computed from the water masks provided with the DEMs and Sentinel-2 Maximum Water Area Extent (MWAE).

Scene	CartoDEM	AW3D30	GLO-30	TanDEM-X DEM
a	54	8	78	68
b	33	3	64	50
c	5	0	11	8
d	9	0	14	10

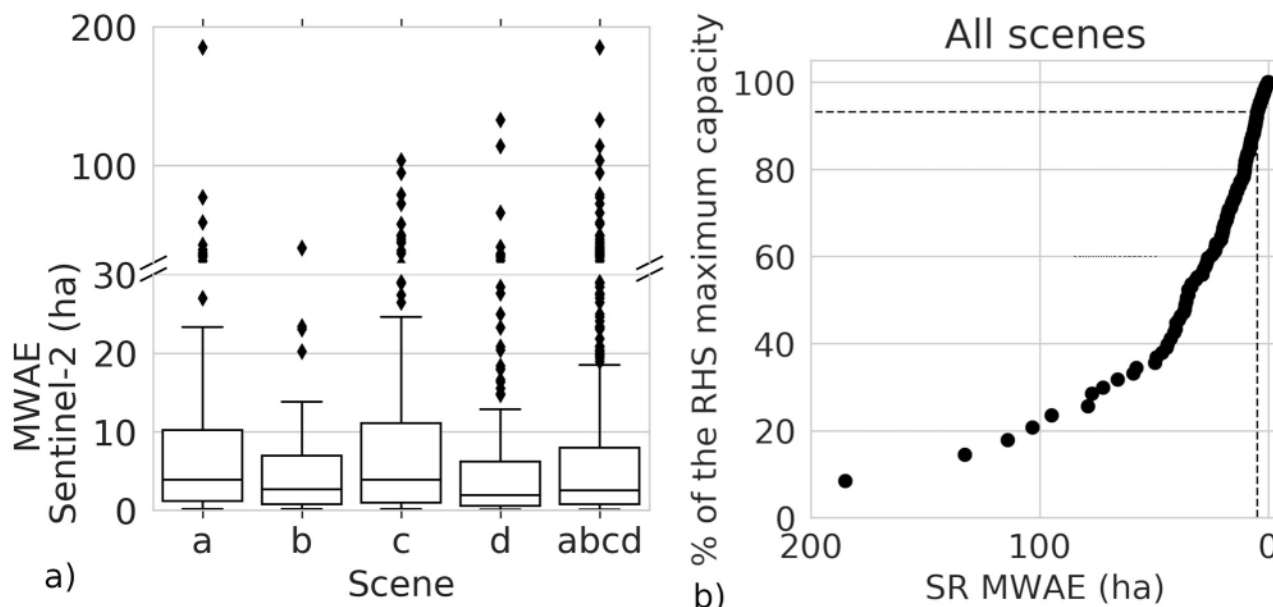https://doi.org/10.1371/journal.pwat.0000260.t003

Fig 6. (a) Distribution (median and quartiles) of Sentinel-2 Maximum Surface Area Extent (MWAE) of the SR per Pléiades scene. (b) Cumulative volumes of the SR of all four Pléiades scenes, in % of the RHS maximum capacity, sorted by decreasing MWAE. SR with an area below 5 ha represents 7% of the RHS maximum capacity (as indicated by the dashed lines).

a 90-m resolution (Pléiades and TanDEM-X) the dike is nearly flattened. The dike and the bathymetry of smaller reservoirs (as the 3 ha reservoir in Fig 7c) are almost completely smoothed at a 30-m resolution. The global slopes are coherent between each source of data, with a absolute bias that does not affect geometries, except for CartoDEM and AW3D30 elevation, that have been rounded to the meter before data dissemination. The maximum capacities of SR larger than 5 ha are underestimated by 5, 10 and 14% for Pléiades resampled at 12, 30 and 90 m, against 10, 26 and 39% for SR smaller than 5 ha.

We quantified the decrease of SR volume estimates from water area extents for large-scale and resampled DEMs. Fig 8 shows an example for a given SR: the series of volumes of GLO-30 and AW3D30 (red and blue points), computed with a 10 cm height increment, are compared with the corresponding water volumes given by the reference hypsometric relationship of Pléiades 2-m DEM (black curve, computed as explained in section 4.1) for the same area. Volumes of individual SR were generally associated with high uncertainties: the median MAPE of SR volumes (shown in Fig 9) over all SR ranges from 43 to 53% for large-scale DEMs, against 22%, 35% and 49% for Pléiades aggregated at 12, 30 and 90 m.

Apart from resolution and numerical precision, another major requirement for bathymetry retrieval and essential for accurate volume estimation is the absence of water in the SR during DEM acquisition. The filling ratio of the four large-scale DEMs, is reported in Table 3. CartoDEM, GLO-30 and TanDEM-X DEM show high (>33%) filling ratios for scenes (a) and (b). AW3D30 is the only DEM with a low filling ratio on the four scenes (<8%).

We examined the impact of this filling ratio on the estimation of the volumes of SR. Fig 10 shows the MAPE of all SR plotted against their individual filling ratio during DEM acquisition for CartoDEM, AW3D30, GLO-30 and TanDEM-X DEM. The estimation error seems to be correlated to the filling ratio for GLO-30 and AW3D30, slightly less for CartoDEM and TanDEM-X DEM. However, a great variability of errors is visible even for empty SR (filling ratio = 0%), in particular for the smaller ones (little dark red dots, often smaller than 5 ha).
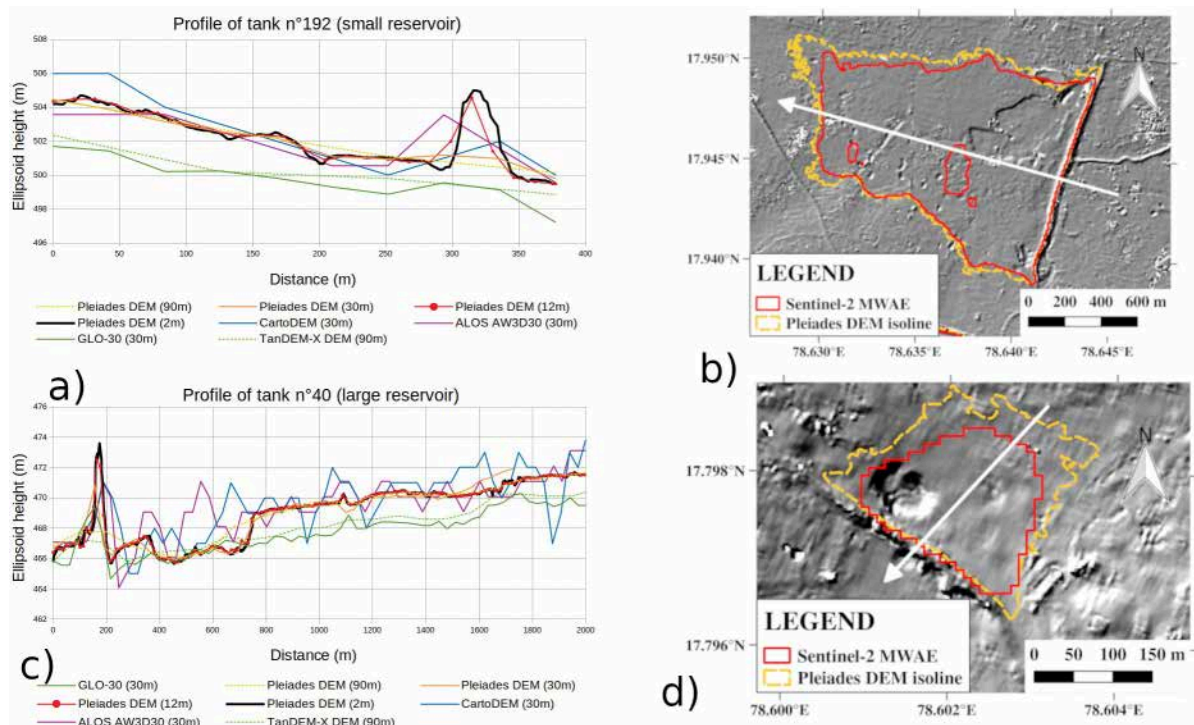
Fig 7. Profiles of 2 SR for Pléiades at 2-m, 12-m, 30- and 90-m resolution, CartoDEM, AW3D30, GLO-30 and TanDEM-X DEM. Both reservoirs were empty during all DEM acquisitions. (a) and (c): Profiles of a large (114 ha) and a small (3 ha) reservoir. y values in vertical axis are ellipsoidal heights referenced to the WGS84-G1150 ellipsoid [56] which is the native projection of Pléiades, CartoDEM and TanDEM-X DEM. AW3D30 and GLO-30 are altitudes referenced to the EGM96 geoid [57] and were converted to ellipsoid height for this figure [58]. (b) and (d): Context of the profile. The map background is Pléiades 2-m DEM hillshade (publicly available 10.5281/zenodo.10403040), the dashed blue line the manually selected Pléiades DEM isoline (publicly available here 10.5281/zenodo.10402355) and the white arrow is the transect.

https://doi.org/10.1371/journal.pwat.0000260.g007

This confirms the inability of these four DEMs to correctly measure the volume of smaller SR because of their coarse resolution.

4.3 Volume retrieval from Sentinel-2 time series at Pléiades scene scale

Sentinel-2 time series were used to estimate the water volume stored in each tank covered by Pléiades DEM at different hydrological period and filling rate. These volumes, estimated with each DEM derived hypsometric relationship, were compared to the reference, i.e volumes from the hypsometric relationships derived from Pléiades 2-m DEM. The average MAPE and MPE computed on the time series of the volumes of individual SR are reported in Table 4 (the MAPE and MPE were computed on the time series for each SR, then averaged). MAPEs are high for large-scale DEMs, ranging from 52% to 188%. Even the resampling of Pléiades DEM at 12 m induces high error, ranging from 22 to 43%. This shows that large-scale DEMs cannot be used to monitor the volume of individual SR. Note that these MAPEs estimated from Sentinel-2 time series are larger than those estimated from all V-A sample points in section 4.2. Indeed, water area extents detected by Sentinel-2 over time are not equally distributed on the V-A relationship as higher areas rarely occur, and small volumes estimates that have the largest relative uncertainty.

However, aggregating individual volumes at the Pléiades scene scale improves their correspondence with volumes derived from Pléiades 2 m DEM. Fig 11 shows lumped volume
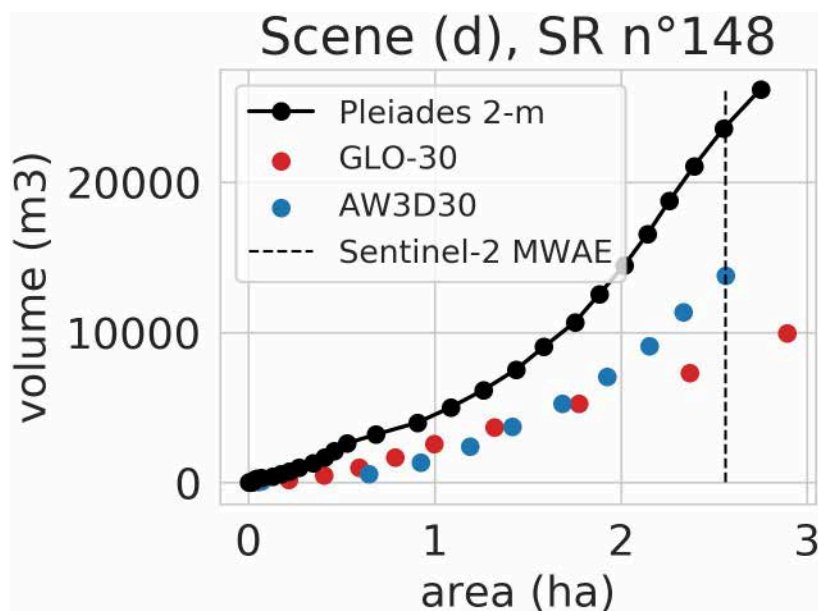
Fig 8. V-A pairs of a SR (2.6 ha) for three DEMs. The hypsometric relationship derived from Pléiades 2-m DEM is in black, linearly interpolated between black dots. Red and blue dots are the V-A pairs of GLO-30 and AW3D30.

estimates from the eight DEMs. Only a subset of the Sentinel-2 time series is shown for better visibility. High values (>100%) of volume relative uncertainty were found for very small areas (<1% of the maximum RHS area). These outliers can dramatically increase MAPE and MPE despite representing a low absolute uncertainty, and were therefore removed from the
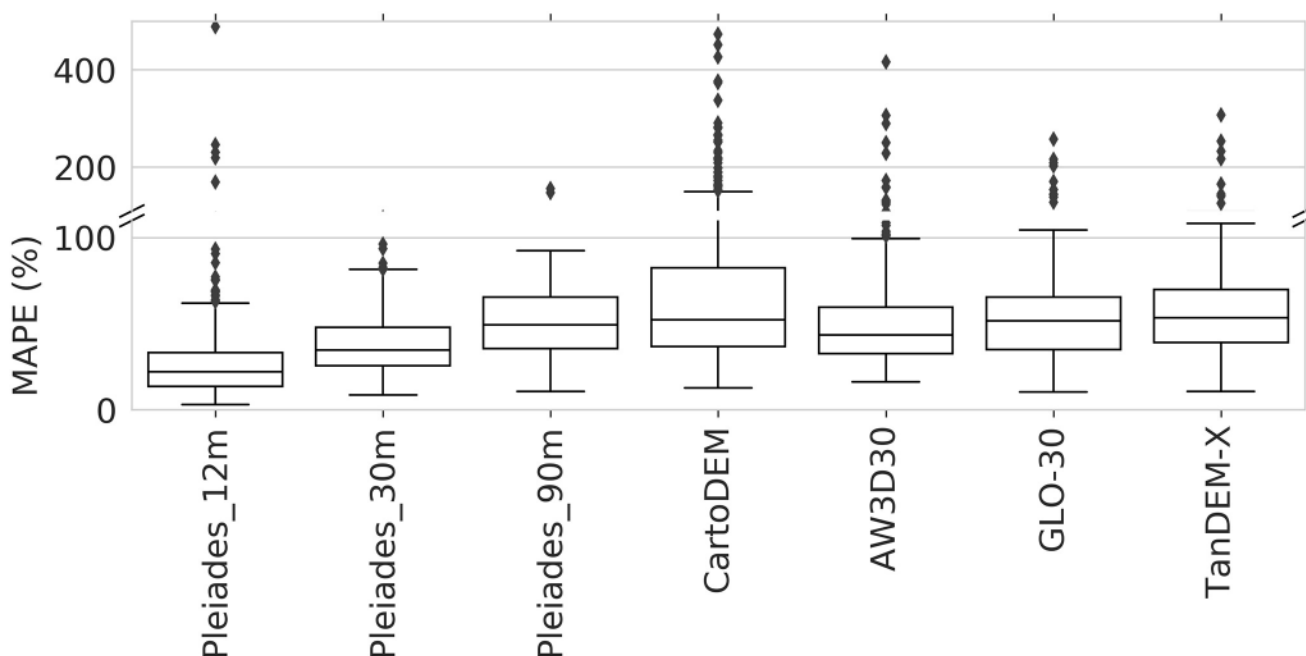
Fig 9. Distribution (median and quartiles), over all small reservoirs (SR), of the mean absolute percentage error (MAPE) of SR volumes extracted from several DEMs at a 10 cm increment, relative to Pléiades 2-m DEM reference volume.
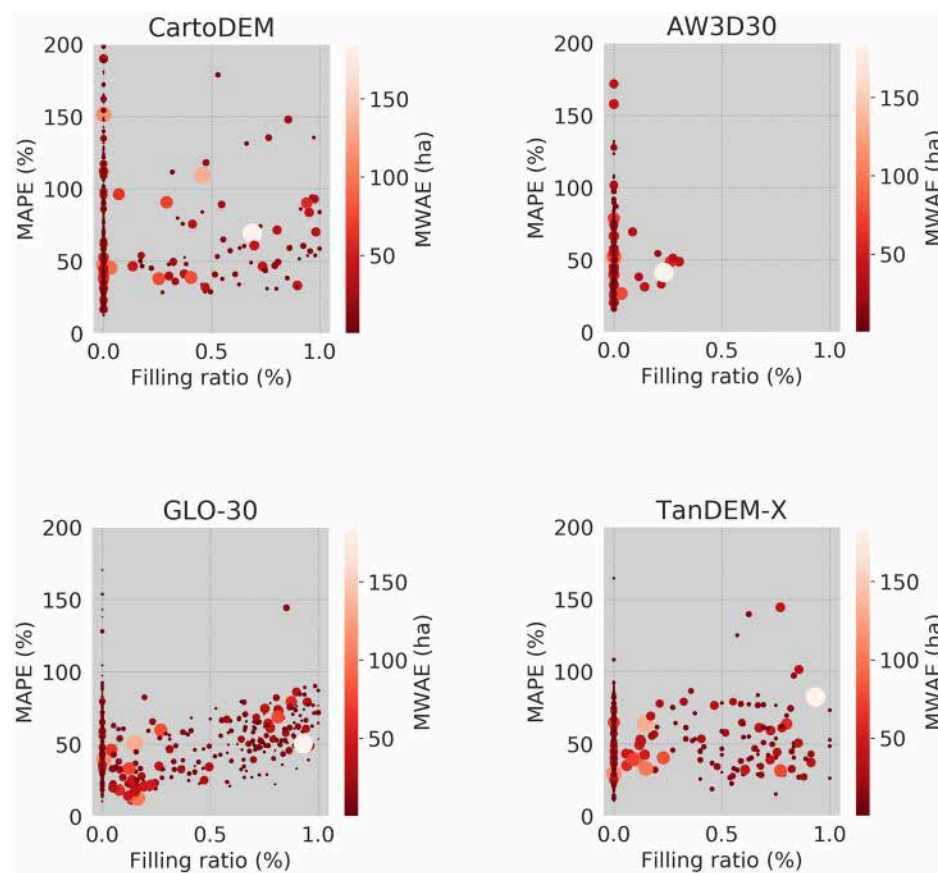
Fig 10. MAPE of small reservoirs (SR) in relation to their filling ratio at the moment of the DEM acquisition.
Each point represents one SR. The color and size of each point correspond to the Sentinel-2 Maximum Water Area Extent (MWAE) of the SR in ha.

https://doi.org/10.1371/journal.pwat.0000260.g010

calculation of the metrics presented in this section (16 points for AW3D30 in scene (c)). The R^2, MAPE and MPE of scene-scale volumes, computed over the time series, are reported in Table 5.

The MAPEs of aggregated values at the Pléiades scene scale are lower than for individual SR (12% against 72%), which shows that the errors on SR compensate each other and the aggregation of small volumes produces better regional volume estimates than with each individual SR.

On the four areas covered by Pléiades acquisitions, volume estimates are less accurate (R^2 decreases) with the reduction of Pléiades resolution (Table 5). As expected, a lower resolution

Table 4. Average MAPE (%) and MPE (%) of volumes computed with Sentinel-2-derived water area extents time series for each SR.

| Image	Pléiades 12m		Pléiades 30m		Pléiades 90m		CartoDEM		AW3D30		GLO-30		TanDEM-X	
	MAPE	MPE	MAPE	MPE	MAPE	MPE	MAPE	MPE	MAPE	MPE	MAPE	MPE	MAPE	MPE
a	22.4	19.9	34.4	27.6	44.5	38.9	108.3	-21.9	52.2	7.7	121.9	-1.6	52.5	21.2
b	30.0	23.8	41.2	32.7	53.1	39.5	123.7	-62.0	57.1	0.7	188.2	-83.4	75.1	17.5
c	43.4	30.2	50.4	47.7	67.7	50.5	72.8	-12.8	58.6	-0.2	106.4	-21.7	65.1	50.3
d	25.7	20.8	41.4	33.4	66.7	43.7	96.3	-37.2	81.2	-4.3	111.6	-25.1	64.9	45.7
all	29.8	23.3	41.9	35.5	60.2	43.8	96.5	-30.5	66.0	0.1	121.6	-25.5	63.2	37.8

https://doi.org/10.1371/journal.pwat.0000260.t004
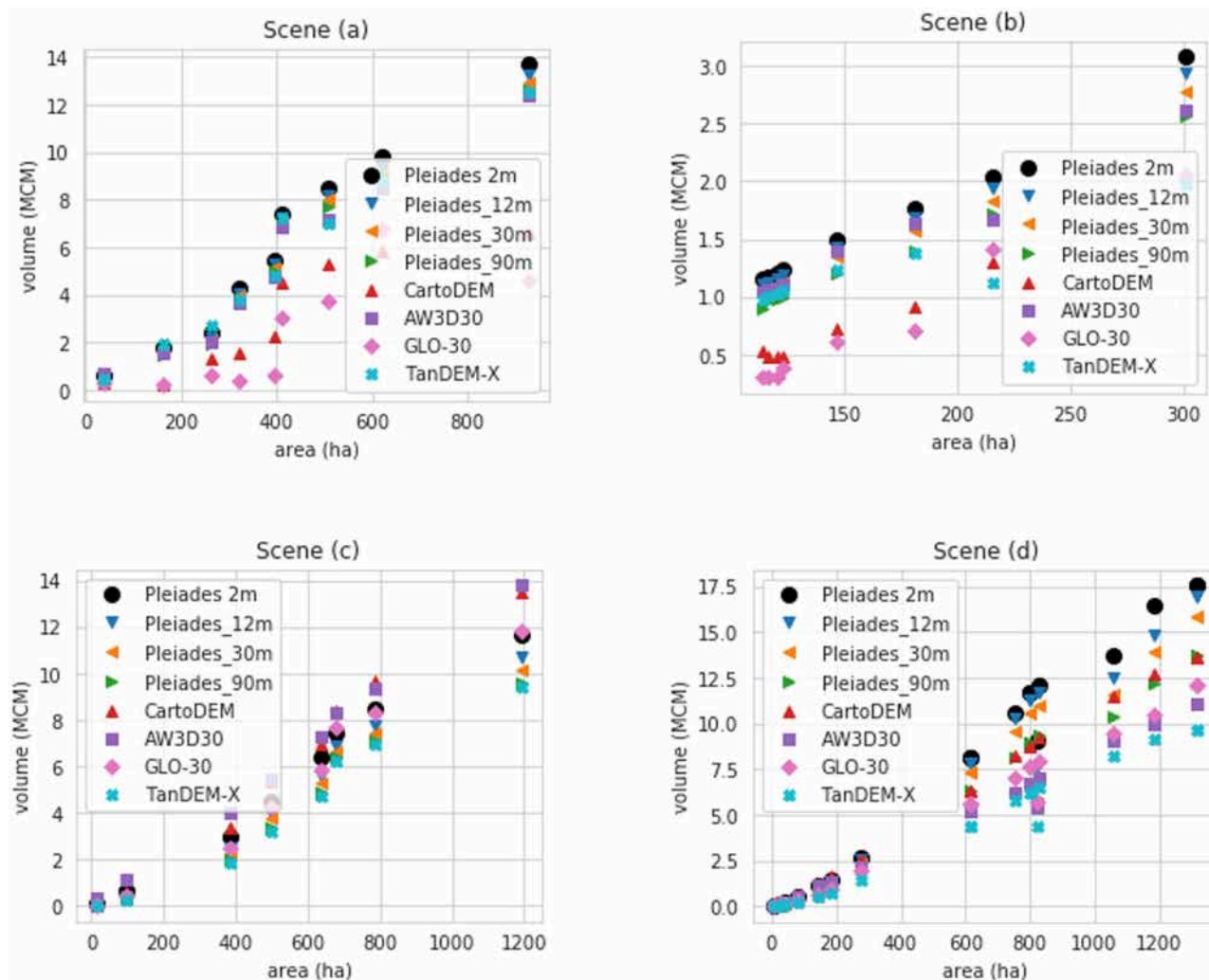
Fig 11. Lumped volume and area for all 4 Pléiades scenes. Only a subset of the time series is plotted. Reference values are black dots.

https://doi.org/10.1371/journal.pwat.0000260.g011

induces a systematic negative bias (MPE>0 and MAPE≃MPE) on the four Pléiades scenes, as the the dikes geometries are flattened. Nevertheless, these bias increase drastically above 30m. Indeed, the relative uncertainty reaches 28% on average for a 30 m resolution.

The filling rate of the RHS, i.e. the percentage of the RHS maximum area covered by surface water at the time of acquisition, is high for CartoDEM, GLO-30 and TanDEM-X (>33%, for

Table 5. R^2 (%), MAPE (%) and MPE (%) of the time series of volumes lumped at scene scale with Sentinel-2 areas. The last line presents the metrics computed on the series of V-A points of all scenes.

Image	Pléiades 12m			Pléiades 30m			Pléiades 90m			CartoDEM			AW3D30			GLO-30			TanDEM-X		
	R^2	MAPE	MPE	R^2	MAPE	MPE	R^2	MAPE	MPE	R^2	MAPE	MPE	R^2	MAPE	MPE	R^2	MAPE	MPE	R^2	MAPE	MPE
a	99.4	4.4	4.4	98.5	7.0	7.0	97.3	10.2	10.1	8.4	57.1	57.1	95.2	11.9	11.1	-54.2	72.1	72.1	95.9	12.3	7.2
b	99.2	18.0	18.0	98.1	29.1	29.1	94.6	43.0	43.0	77.3	48.4	48.4	97.4	26.1	20.0	70.1	69.1	69.1	83.7	36.9	36.9
c	97.4	28.0	28.0	95.2	37.9	37.9	91.9	46.6	46.6	96.2	18.8	5.4	95.9	20.6	-12.5	98.8	28.5	28.2	90.5	47.9	47.9
d	99.4	10.2	10.2	97.8	29.4	29.4	91.9	44.3	44.3	93.4	15.3	-5.9	80.3	16.3	7.7	85.0	38.4	38.4	71.8	57.2	57.2
all	99.0	16.2	16.2	97.5	28.1	28.1	94.0	38.6	38.6	81.7	29.0	17.4	90.0	18.2	4.6	69.1	45.8	45.7	85.2	42.8	41.9

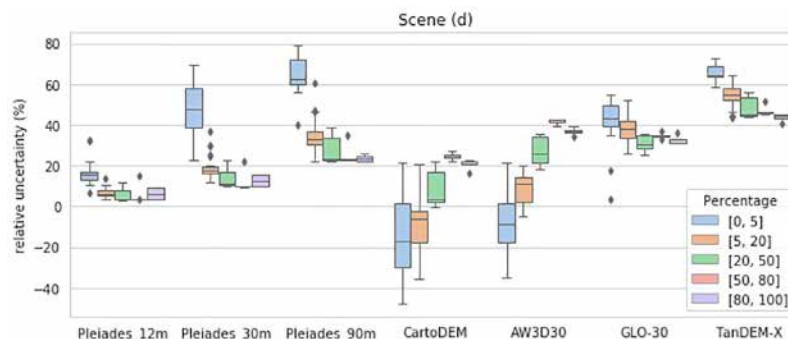https://doi.org/10.1371/journal.pwat.0000260.t005

Fig 12. Relative uncertainty of volume estimates at scene scale for scene (d). The V-A points of the time series of all four scenes are gathered by their proportion of surface water area relative to the maximum area of the RHS of scene (d).

scenes (a) and (b), Table 3), which impacts their performances compare to AW3D30 (filling ratio<8%). GLO-30 has the largest filling ratio (78% and 64% for scenes (a) and (b)) and the least accurate estimates (Table 5) with R^2 = -54% and 70% for scenes (a) and (b). Fig 11 shows that those DEM lead to large underestimation of volumes and thus are not suitable for RHS volume monitoring in this region. TanDEM-X DEM performs better than CartoDEM (higher R^2) despite its lower resolution and higher filling ratio. AW3D30 volume estimates are similar to those of the reference Pléiades DEM resampled at 30-m for scenes (a) and (b), i.e. it can be used at the Telangana scale taking the bias presented in this study into account.

On scenes (c) and (d) the filling ratio is lower than 11% for all DEM. CartoDEM, AW3D30 and GLO-30 estimates are relatively good (R^2 from 80 to 99%). The coarser TanDEM-X DEM produces the least accurate volume estimates. GLO-30 produces the best estimates for image (c) (R^2=98.8%) among all DEMs including Pléiades resampled at 30-m, and CartoDEM performs better than the three other large-scale DEMs and Pléiades 30-m for image (d) (R^2=96.5%), despite the fact that AW3D30 has the lower filling ratio for these two scenes.

For almost all scenes and DEMs, volumes are generally estimated with a negative bias, except for CartoDEM and AW3D30 in scene (c) and (d), for which the MPE can even be negative.

Volume estimates have different accuracies for low and high filling rates. Relative uncertainties reaches their maximum (80% and -50%) for smallest water area extent (<5% of the total RHS surface area) and decreases for higher filling rates (Fig 12). Contrary to resampled Pléiades DEM, GLO-30 and TanDEM-X DEM, for which increasing volumes are estimated with a decreasing negative bias, CartoDEM and AW3D30 overestimate low volumes and underestimate large one.

5 Discussion

Could any global DEM tested in this study being used to get a proxy of water volume stored in the RHS as a function of the surface water mask derived from satellites? In the following, we discuss the SR volume retrieval errors from surface water detection time series from Sentinel-2 and global available DEM over the study area. The discussion is about the benefit or uselessness for hydrologists and water management institutions to extract water volume stored in this ungauged hydrological system during the 8 months of dry season. The main factors impacting the retrieval accuracy are discussed: surface water extent accuracy, DEM accuracy, DEM spatial and numerical resolution, SR filling ratio and size.

5.1 Pléiades DEM accuracy

The accuracy of Pléiades DEM at 2m was evaluated using existing Lidar elevation measurement from IceSAT-2 mission. This very limited comparison confirms that the DEM produced have a regional coherence with ICESAT-2, but is not sufficient to establish the DEM as a "ground truth". We rather consider this DEM as the reference to estimate the relative errors of the other DEM generated at coarser resolutions (at 12, 30 and 90m) and global DEM products. Absolute errors would require further in situ validation, based on total station measurements or drone acquisitions. This study shows that relative elevation from stereoscopy at very high (2m) and high resolution (12m) is able to monitor the storage capacity of the Indian RHS. NMAD remains lower to 60cm between data-sets (see Table 2) and even aggregated at 12m, dikes height are enough precise (see Fig 7 to limit the aggregated volume MAPE errors to 20% (see Table 4). This 12m resolution produced from a higher resolution could be the resolution of the distributed DEM product to the users for instance.

5.2 Surface water extent accuracy

Sentinel-2, as a multispectral data at 10 to 20 m resolution is well adapted to the size of the main SR of the RHS. Nevertheless, it is also known to underestimate surface water area extent especially for seasonal shallow temporary lakes, with a non negligible erosion of water extent on the SR edges or caused by floating vegetation [59]. The comparison of Sentinel-2-derived water maps with higher resolution images (as explained in section 3.2.2) showed an average negative bias on volume estimates: the average relative error (MAPE) was estimated at 17% on water area extents and 31% on volumes, which is in accordance with the 15% negative bias found in [60]. This bias could be reduced by detecting water on optical images with a higher spatial resolution than Sentinel-2, such as Venµs (5.3 m resolution, 2 days revisit time, but not global) [61] or Planet (3m resolution, daily revisit but commercial) [62]. However, the use of optical images only allows the retrieval of a partial time series because of missing images during cloudy periods. Radar observations such as those from Radarsat-2, TanDEM-X, or Sentinel-1 can provide dense time series but underestimate surface water coverage. Previous studies quantified that using Sentinel-1 data rather than optical data could underestimate reservoirs water areas by 15% [18] and water volumes by 27% [26] in the RHS located in Tamil-Nadu state (India). We chose to use water maps produced from Sentinel-2 optical images, to get a realistic example of water volume retrieval dynamic Fig 10 rather than generating random surface water area extents for each SR.

5.3 Hypsometry relationship

The construction of individual V-A relationship relies on a vertical subsampling of each DEM. This can be challenging for (i) coarse DEMs for which the number of pixels by SR is low, (ii) DEMs rounded to the meter, (iii) DEMs for which the depth of SR is lowered by the presence of water at the time of acquisition. The bilinear resampling of DEMs at a finer resolution (2-m in this study) allows a better vertical sampling by solving issues (i) and (ii). The density of V-A points remains nonetheless inferior for large-scale DEMs than for Pléiades 2-m DEM (as illustrated in Fig 8), producing a "sparser" hypsometric curve and reducing the accuracy of volume estimation from Sentinel-2 images. Previous studies of medium to large dams have used various methods to extrapolate water volume below the water surface detected by satellite data-based DEMs [28]. We have chosen not to apply such extrapolation to avoid mixing sources of uncertainties in the analysis. But the presence of water behind each DEM is shown in the Table 3, expressed as a "filling ratio". From the Table 3, the AW3D30 is the DEM with the least surface water at the time of its acquisition.

5.4 Heterogeneous negative bias of volume restitution from freely available DEMs

Surface water Volume estimates depend on (i) the spatial resolution of the DEM, (ii) the SR filling rate during its acquisition and (iii) its numerical precision (float or integer format). Underestimation comes with low resolution and high filling ratio at the time of acquisition: up to 72% at scene scale with a filling ratio of 78% for GLO-30. On the contrary, DEMs distributed in Integer format induces unpredictable uncertainties. The systematic negative bias due to coarse resolution can be compensated by upward rounding errors, which eventually and incidentally decrease volume estimates errors at the scene level. Volume estimates from Carto-DEM and AW3D30 are occasionally better than Pléiades 30-m DEM for this reason.

The long period between DEMs acquisition dates can also impact volume estimates. Natural sediment depositions vs SR rejunevation public policies have modeled dikes and bathymetry as seen in Fig 4c. Rejuvenation activities consist in desiltation to increase aquifer recharge and dike rise to increase storage capacity (the state program Kakatiya project in 2015 and the federal mission Amrit Sarovar in 2022). It should be relevant to monitor those changes at least once in a decade with new VHR DEM acquisitions during dry months to update SR bathymetries and monitor new ones. Note that we chose not to include in this study the DEM from the Shuttle Radar Topography Mission (SRTM) [63] based on 2000 acquisitions, that we estimated too ancient and obsolete regarding the RHS observed with Pléiades acquisitions (16 and 19 years after) given those recent changes that occurred in the study area.

5.5 SR delineation

As presented in section 3.2.3, the hypsometry retrieval process is highly dependent on the agreement between SR limits and the DEM isolines. The use of optical satellite data such as Sentinel-2-derived MWAE (Maximum Water Area Extent) for SR delineation is a fast semi-automatic process. Nevertheless, the discrepancy discussed before between the surface water area extents and Pléiades DEM isolines imposes to manually delineate SR with Pléiades DEM isoline, a time-consuming task that can not be reproduced at large scales. This task was fully automated in [29, 64] by using a Blue Spot detection algorithm, which identifies natural depressions. In particular, [29] used this method in the Cuvelai Basin, a semi-arid area flooded part of the year, to determine a high resolution theoretical MWAE of natural depressions that were measured using TanDEM-X DEM commercial product at 12-m resolution and estimated their potential water storage. A combination of the Blue Spot detection algorithm and surface water maps derived from Sentinel-2 could be a solution for the automatic retrieval of active SR MWAE limits.

5.6 Monitoring the RHS of Telangana: What DEM and what uncertainty?

This study shows that VHR DEM resampled at 12 or 30 m enables to estimate water volumes from surface water area with an error (i.e. MAPE computed with the native 2 m resolution as a reference) less than 16 and 28% at the scale of the study area, with higher errors for lowest volumes and smallest water bodies. This error ranges from 18 to 45% for the large-scale DEMs. On the other hand, the quantification of the 15 main largest and highly filled SR of the RHS would enable to quantify 40% of this potential water resource (Fig 6b). This can be particularly relevant as the volume of these largest reservoirs can represent a higher portion of the RHS volume during the dry season, as the largest reservoirs are generally the last ones to empty. At regional scale, this amount of water is small compare to the groundwater and large dams

resources, but remain important for local farmers in upstream areas disconnected from the main large rivers and dams.

6 Conclusions and perspectives

This study draws some perspectives about the nowadays and foreseen space-borne datasets and products that could be used by hydrologists to monitor the water storage within the Indian RHS. The small reservoirs (SR) composing the Rainwater Harvesting System (RHS) are a crucial water resource for irrigation and livestock in upstream rural areas in South India. They are also crucial to understand the impact of the RHS on the water cycle (including groundwater additional recharge) in these semi-arid areas, and their dimensions crucial to hydrological modeling approaches [65]. We used the bathymetry from a 2-m Digital Elevation Model (DEM) over a 1,800 km^2 area to derive volume-area relationships for more than 500 SR. Times series of Sentinel-2-derived surface water area over several years were used to simulate several filling rates of the RHS and compute volume estimates at larger scales. We have been able to cover a maximal resource capacity of 47 million cubic meters over the four Pléiades stereoscopic acquisitions (Fig 11). We used these 2m DEM based hypsometric relationship as a virtual reference to quantify the relative errors of RHS volume retrieval at 12, 30 and 90 meters, and from 3 large-scale DEMs at 30-m resolution (AW3D30, GLO-30, CartoDEM) and one DEM at 90-m resolution (TanDEM-X DEM). These four areas covered by this study are representative of the RHS in term of Small Reservoirs size diversity and spatial density found in the Telangana state (see the dataset [66]). Nevertheless, no generalization of the SR geometries and Volume surface relationship has been found with the 500. There is a need to extract SR geometries using stereoscopy everywhere at the appropriate time.

Volume estimates at SR scale were associated with high relative uncertainties, ranging from 47% to 78% for large-scale DEMs against 17%, 29% and 46% for Pléiades DEM aggregated at 12, 30 and 90 m. Volume estimates lumped at larger scale have better accuracies because of the compensation of the uncertainties of individual SR. We found that at scene scale, the Pléiades DEM at 12-m resolution could estimate the RHS volume with a R^2 from 97.4% to 99.4% and a MAPE (Mean Absolute Percentage Error) from 4% to 28%, but with higher uncertainties in dry conditions (low RHS filling rates). The Pléiades DEM aggregated at 30-m was able to estimate the RHS volume at scene scale with a R^2 from 95.2 to 98.5% and a MAPE from 7 to 38%. However, volumes are estimated with a quasi-systematic negative bias when the resolution decreases due to (i) the underestimation of the volume of very small reservoirs (<5ha) that are hardly visible by larger DEM and (ii) the smoothing of the SR geometry. The use of a 90-m resolution DEM degrades volume estimates even more, and we recommend using a resolution no coarser than 30 meters and to focus on the largest SR composing the major part of the RHS volume in this region.

Results indicate that the acquisition period of DEM is crucial, i.e. the filling ratio of the RHS at the time of acquisition. AW3D30 had the lowest RHS filling ratio of all DEM (<6% on all 4 scenes) and hence showed the best results on average over the 4 scenes (R^2 from 80.3 to 97.4% and MAPE from 8 to 26%). On the other hand, CartoDEM and GLO-30 were able to produce better results at scene scale for a low filling ratio (<10%). In absence of VHR DEMs, the best strategy is to use a 30-m global DEM acquired recently, or a combination of several DEM with a low filling ratio (<10%) covering the study area, to approximate the volume of the RHS at regional scale from time series of surface water maps. Yet an average relative error of about 26% can be expected following our results shown in Table 5 for AW3D30. These results should be taken with caution as we have had the opportunity to sample less than 2% of the Telangana area. However, at very local or SR scale, or for low water stocks, high-resolution

DEMs are essential to estimate and monitor surface water storage with precision in near-real time in combination with high resolution optical observations. IceSAT-2 ATL03 dataset has also proved its ability to retrieve some information about the size (height and width) of dykes. Nevertheless, its spatial sampling and revisit is not adequat to monitor the RHS. The need for large scale inland water bodies monitoring has motivated the forthcoming SWOT (Surface Water and Ocean Topography) mission [67], yet its sensitivity to small water bodies need to be verified, in particular those with an area below 5 ha. Will SWOT detect accurately this hydrological system in term of surface and elevation? The question is still open.

7 Financial disclosure

Author Contributions

Conceptualization: Claire Pascal, Sylvain Ferrant.

Data curation: Claire Pascal, Taeken Wijmer.

Formal analysis: Sylvain Ferrant, Simon Gascoin.

Funding acquisition: Sylvain Ferrant, Olivier Merlin.

Investigation: Claire Pascal, Sylvain Ferrant, Olivier Merlin.

Methodology: Claire Pascal, Sylvain Ferrant, Taeken Wijmer.

Project administration: Sylvain Ferrant.

Software: Santiago Peña-Luque, Simon Gascoin.

Supervision: Sylvain Ferrant, Olivier Merlin.

Validation: Sylvain Ferrant.

Visualization: Claire Pascal, Sylvain Ferrant, Santiago Peña-Luque, Adrien Selles, Simon Gascoin.

Writing – original draft: Claire Pascal, Sylvain Ferrant.

Writing – review & editing: Sylvain Ferrant, Santiago Peña-Luque, Adrien Selles, Jean-Christophe Marechal, Simon Gascoin, Olivier Merlin.

References

1. Wada Y, Beek LPHv, Viviroli D, Dürr HH, Weingartner R, Bierkens MFP. Global monthly water stress: 2. Water demand and severity of water stress. Water Resources Research. 2011; 47(7). https://doi.org/10.1029/2010WR009792

2. Habets F, Molénat J, Carluer N, Douez O, Leenhardt D. The cumulative impacts of small reservoirs on hydrology: A review. Science of The Total Environment. 2018; 643:850–867. https://doi.org/10.1016/j.scitotenv.2018.06.188 PMID: 30189581

3. Krol MS, de Vries MJ, van Oel PR, de Araújo JC. Sustainability of Small Reservoirs and Large Scale Water Availability Under Current Conditions and Climate Change. Water Resources Management. 2011; 25(12):3017–3026. https://doi.org/10.1007/s11269-011-9787-0

4. Sakthivadivel R. The groundwater recharge movement in India. In: Giordano M, Villholth KG, editors. The Agricultural Groundwater Revolution: Opportunities and Threats to Development. Comprehensive Assessment of Water Management in Agriculture Series. Wallingford, United Kingdom: CABI Publishing; 2007.

5. Glendenning CJ, van Ogtrop FF, Mishra AK, Vervoort RW. Balancing watershed and local scale impacts of rain water harvesting in India—A review. Agricultural Water Management. 2012; 107:1–13. https://doi.org/10.1016/j.agwat.2012.01.011

6. Boisson A, Baïsset M, Alazard M, Perrin J, Villesseche D, Dewandel B, et al. Comparison of surface and groundwater balance approaches in the evaluation of managed aquifer recharge structures: Case of a percolation tank in a crystalline aquifer in India. Journal of Hydrology. 2014; 519:1620–1633. https://doi.org/10.1016/j.jhydrol.2014.09.022

7. Massuel S, Perrin J, Mascre C, Mohamed W, Boisson A, Ahmed S. Managed aquifer recharge in South India: What to expect from small percolation tanks in hard rock? Journal of Hydrology. 2014; 512:157–167. https://doi.org/10.1016/j.jhydrol.2014.02.062

8. Perrin J, Ferrant S, Massuel S, Dewandel B, Maréchal JC, Aulong S, et al. Assessing water availability in a semi-arid watershed of southern India using a semi-distributed model. Journal of Hydrology. 2012; 460-461:143–155. https://doi.org/10.1016/j.jhydrol.2012.07.002

9. Baup F, Frappart F, Maubant J. Combining high-resolution satellite images and altimetry to estimate the volume of small lakes. Hydrology and Earth System Sciences. 2014; 18(5):2007–2020. https://doi.org/10.5194/hess-18-2007-2014

10. Crétaux JF, Arsen A, Calmant S, Kouraev A, Vuglinski V, Bergé-Nguyen M, et al. SOLS: A lake database to monitor in the Near Real Time water level and storage variations from remote sensing data. Advances in Space Research. 2011; 47(9):1497–1507. https://doi.org/10.1016/j.asr.2011.01.004

11. Duan Z, Bastiaanssen WGM. Estimating water volume variations in lakes and reservoirs from four operational satellite altimetry databases and satellite imagery data. Remote Sensing of Environment. 2013; 134:403–416. https://doi.org/10.1016/j.rse.2013.03.010

12. Frappart F, Minh KD, L'Hermitte J, Cazenave A, Ramillien G, Le Toan T, et al. Water volume change in the lower Mekong from satellite altimetry and imagery data. Geophysical Journal International. 2006; 167(2):570–584. https://doi.org/10.1111/j.1365-246X.2006.03184.x

13. de Fleury M, Kergoat L, Grippa M. Hydrological regime of Sahelian small waterbodies from combined Sentinel-2 MSI and Sentinel-3 Synthetic Aperture Radar Altimeter data. Hydrology and Earth System Sciences. 2023; 27(11):2189–2204. https://doi.org/10.5194/hess-27-2189-2023

14. Pekel JF, Cottam A, Gorelick N, Belward AS. High-resolution mapping of global surface water and its long-term changes. Nature. 2016; 540(7633):418–422. https://doi.org/10.1038/nature20584 PMID: 27926733

15. Pickens AH, Hansen MC, Hancher M, Stehman SV, Tyukavina A, Potapov P, et al. Mapping and sampling to characterize global inland water dynamics from 1999 to 2018 with full Landsat time-series. Remote Sensing of Environment. 2020; 243:111792. https://doi.org/10.1016/j.rse.2020.111792

16. Cordeiro MCR, Martinez JM, Peña-Luque S. Automatic water detection from multidimensional hierarchical clustering for Sentinel-2 images and a comparison with Level 2A processors. Remote Sensing of Environment. 2021; 253:112209. https://doi.org/10.1016/j.rse.2020.112209

17. Martinis S, Plank S, Ćwik K. The Use of Sentinel-1 Time-Series Data to Improve Flood Monitoring in Arid Areas. Remote Sensing. 2018; 10(4):583. https://doi.org/10.3390/rs10040583

18. Peña-Luque S, Ferrant S, Cordeiro MCR, Ledauphin T, Maxant J, Martinez JM. Sentinel-1&2 Multitemporal Water Surface Detection Accuracies, Evaluated at Regional and Reservoirs Level. Remote Sensing. 2021; 13(16):3279. https://doi.org/10.3390/rs13163279

19. Tachikawa T, Hato M, Kaku M, Iwasaki A. Characteristics of ASTER GDEM version 2. In: 2011 IEEE International Geoscience and Remote Sensing Symposium; 2011. p. 3657–3660.

20. Krieger G, Zink M, Bachmann M, Bräutigam B, Schulze D, Martone M, et al. TanDEM-X: A radar interferometer with two formation-flying satellites. Acta Astronautica. 2013; 89:83–98. https://doi.org/10.1016/j.actaastro.2013.03.008

21. Tadono T, Ishida H, Oda F, Naito S, Minakawa K, Iwamoto H. Precise Global DEM Generation by ALOS PRISM. In: ISPRS Annals of the Photogrammetry, Remote Sensing and Spatial Information Sciences. vol. II-4. Copernicus GmbH; 2014. p. 71–76.

22. Bonnema M, Hossain F. Inferring reservoir operating patterns across the Mekong Basin using only space observations. Water Resources Research. 2017; 53(5):3791–3810. https://doi.org/10.1002/2016WR019978

23. Li Y, Gao H, Jasinski MF, Zhang S, Stoll JD. Deriving High-Resolution Reservoir Bathymetry From ICE-Sat-2 Prototype Photon-Counting Lidar and Landsat Imagery. IEEE Transactions on Geoscience and Remote Sensing. 2019; 57(10):7883–7893. https://doi.org/10.1109/TGRS.2019.2917012

24. Avisse N, Tilmant A, Müller MF, Zhang H. Monitoring small reservoirs' storage with satellite remote sensing in inaccessible areas. Hydrology and Earth System Sciences. 2017; 21(12):6445–6459. https://doi.org/10.5194/hess-21-6445-2017

25. Bhagwat T, Klein I, Huth J, Leinenkugel P. Volumetric Analysis of Reservoirs in Drought-Prone Areas Using Remote Sensing Products. Remote Sensing. 2019; 11(17):1974. https://doi.org/10.3390/rs11171974

26. Vanthof V, Kelly R. Water storage estimation in ungauged small reservoirs with the TanDEM-X DEM and multi-source satellite observations. Remote Sensing of Environment. 2019; 235:111437. https://doi.org/10.1016/j.rse.2019.111437

27. Magome J, Ishidaira H, Takeuchi K. Method for satellite monitoring of water storage in reservoirs for efficient regional water management. In: Bloschl G, Franks S, Kumagai M, Musiake K, Rosbjerg D, editors. Water Resources Systems-Hydrological Risk, Management and Development. Wallingford: Int Assoc Hydrological Sciences; 2003. p. 303–310.

28. Liu K, Song C, Wang J, Ke L, Zhu Y, Zhu J, et al. Remote Sensing-Based Modeling of the Bathymetry and Water Storage for Channel-Type Reservoirs Worldwide. Water Resources Research. 2020; 56 (11):e2020WR027147. https://doi.org/10.1029/2020WR027147

29. Arendt R, Reinhardt-Imjela C, Schulte A, Faulstich L, Ullmann T, Beck L, et al. Natural Pans as an Important Surface Water Resource in the Cuvelai Basin—Metrics for Storage Volume Calculations and Identification of Potential Augmentation Sites. Water. 2021; 13(2):177. https://doi.org/10.3390/w13020177

30. Pascal C, Ferrant S, Selles A, Maréchal JC, Gascoin S, Merlin O. High-Resolution Mapping of Rainwater Harvesting System Capacity from Satellite Derived Products in South India. In: 2021 IEEE International Geoscience and Remote Sensing Symposium IGARSS; 2021. p. 7011–7014.

31. Gleyzes MA, Perret L, Kubik P. PLEIADES SYSTEM ARCHITECTURE AND MAIN PERFORMANCES. The International Archives of the Photogrammetry, Remote Sensing and Spatial Information Sciences. 2012; XXXIX-B1:537–542. https://doi.org/10.5194/isprsarchives-XXXIX-B1-537-2012

32. Lebègue L, Cazala-Hourcade E, Languille F, Artigues S, Melet O. CO3D, A WORLDWIDE ONE ONE-METER ACCURACY DEM FOR 2025. In: ISPRS—International Archives of the Photogrammetry, Remote Sensing and Spatial Information Sciences. vol. XLIII-B1-2020. Copernicus GmbH; 2020. p. 299–304.

33. Ferrant S, Selles A, Le Page M, Herrault PA, Pelletier C, Al-Bitar A, et al. Detection of Irrigated Crops from Sentinel-1 and Sentinel-2 Data to Estimate Seasonal Groundwater Use in South India. Remote Sensing. 2017; 9(11):1119. https://doi.org/10.3390/rs9111119

34. Ferrant S, Selles A, Le Page M, AlBitar A, Mermoz S, Gascoin S, et al. SENTINEL-1&2 FOR NEAR REAL TIME CROPPING PATTERN MONITORING IN DROUGHT PRONE AREAS. APPLICATION TO IRRIGATION WATER NEEDS IN TELANGANA, SOUTH-INDIA. The International Archives of the Photogrammetry, Remote Sensing and Spatial Information Sciences. 2019; XLII-3/W6:285–292. https://doi.org/10.5194/isprs-archives-XLII-3-W6-285-2019

35. Maréchal JC, Dewandel B, Ahmed S, Galeazzi L, Zaidi FK. Combined estimation of specific yield and natural recharge in a semi-arid groundwater basin with irrigated agriculture. Journal of Hydrology. 2006; 329(1):281–293. https://doi.org/10.1016/j.jhydrol.2006.02.022

36. Lehner B, Liermann CR, Revenga C, Vörösmarty C, Fekete B, Crouzet P, et al. High-resolution mapping of the world's reservoirs and dams for sustainable river-flow management. Frontiers in Ecology and the Environment. 2011; 9(9):494–502. https://doi.org/10.1890/100125

37. Beyer R, Alexandrov O, ScottMcMichael. NeoGeographyToolkit/StereoPipeline: ASP 2.6.2; 2019.

38. Marti R, Gascoin S, Berthier E, de Pinel M, Houet T, Laffly D. Mapping snow depth in open alpine terrain from stereo satellite imagery. The Cryosphere. 2016; 10(4):1361–1380. https://doi.org/10.5194/tc-10-1361-2016

39. Shean DE, Alexandrov O, Moratto ZM, Smith BE, Joughin IR, Porter C, et al. An automated, open-source pipeline for mass production of digital elevation models (DEMs) from very-high-resolution commercial stereo satellite imagery. ISPRS Journal of Photogrammetry and Remote Sensing. 2016; 116:101–117. https://doi.org/10.1016/j.isprsjprs.2016.03.012

40. Neuenschwander KLPBPJJRJMSCPRFNDHDPBK A L, Sheridan R. ATLAS/ICESat-2 L3A Land and Vegetation Height, Version 6; 2023. Available from: https://nsidc.org/data/ATL08/versions/6.

41. Neumann ABDHJRAGJLKHJSSBL T A, Rebold T. ATLAS/ICESat-2 L2A Global Geolocated Photon Data, Version 6; 2023. Available from: https://nsidc.org/data/ATL03/versions/6.

42. Muralikrishnan S, Narender B, Reddy S, Pillai A. Evaluation of Indian National DEM from Cartosat-1 Data; 2011.

43. Wessel B. TanDEM-X DEM Product Specification; 2016.

44. Takaku J, Tadono T, Tsutsui K. Generation of High Resolution Global DSM from ALOS PRISM. The International Archives of the Photogrammetry, Remote Sensing and Spatial Information Sciences. 2014; XL-4:243–248. https://doi.org/10.5194/isprsarchives-XL-4-243-2014

45. Hagolle O, Huc M, Desjardins C, Auer S, Richter R. MAJA Algorithm Theoretical Basis Document. 2017. https://doi.org/10.5281/zenodo.1209633

46. Nobre AD, Cuartas LA, Hodnett M, Rennó CD, Rodrigues G, Silveira A, et al. Height Above the Nearest Drainage—a hydrologically relevant new terrain model. Journal of Hydrology. 2011; 404(1):13–29. https://doi.org/10.1016/j.jhydrol.2011.03.051

47. Yamazaki D, Ikeshima D, Sosa J, Bates PD, Allen GH, Pavelsky TM. MERIT Hydro: A High-Resolution Global Hydrography Map Based on Latest Topography Dataset. Water Resources Research. 2019; 55 (6):5053–5073. https://doi.org/10.1029/2019WR024873

48. Höhle J, Höhle M. Accuracy assessment of digital elevation models by means of robust statistical methods. ISPRS Journal of Photogrammetry and Remote Sensing. 2009; 64(4):398–406. https://doi.org/10.1016/j.isprsjprs.2009.02.003

49. Zhong J, Liu X, Shen X, Jiang L. A Robust Algorithm for Photon Denoising and Bathymetric Estimation Based on ICESat-2 Data. Remote Sensing. 2023; 15(8). https://doi.org/10.3390/rs15082051

50. Breiman L. Random Forests. Machine Learning. 2001; 45(1):5–32. https://doi.org/10.1023/A:1010933404324

51. Tulbure MG, Broich M, Stehman SV, Kommareddy A. Surface water extent dynamics from three decades of seasonally continuous Landsat time series at subcontinental scale in a semi-arid region. Remote Sensing of Environment. 2016; 178:142–157. https://doi.org/10.1016/j.rse.2016.02.034

52. Bangira T, Alfieri SM, Menenti M, van Niekerk A. Comparing Thresholding with Machine Learning Classifiers for Mapping Complex Water. Remote Sensing. 2019; 11(11):1351. https://doi.org/10.3390/rs11111351

53. McFeeters SK. The use of the Normalized Difference Water Index (NDWI) in the delineation of open water features. International Journal of Remote Sensing. 1996; 17(7):1425–1432. https://doi.org/10.1080/01431169608948714

54. Xu H. Modification of normalised difference water index (NDWI) to enhance open water features in remotely sensed imagery. International Journal of Remote Sensing. 2006; 27(14):3025–3033. https://doi.org/10.1080/01431160600589179

55. Rodrigues LN, Sano EE, Steenhuis TS, Passo DP. Estimation of Small Reservoir Storage Capacities with Remote Sensing in the Brazilian Savannah Region. Water Resources Management. 2012; 26 (4):873–882. https://doi.org/10.1007/s11269-011-9941-8

56. Gruber A, Wessel B, Martone M, Roth A. The TanDEM-X DEM Mosaicking: Fusion of Multiple Acquisitions Using InSAR Quality Parameters. IEEE Journal of Selected Topics in Applied Earth Observations and Remote Sensing. 2016; 9(3):1047–1057. https://doi.org/10.1109/JSTARS.2015.2421879

57. Lemoine FGK. The Development of the Joint NASA GSFC and the National Imagery and Mapping Agency (NIMA) Geopotential Model EGM96; 1998.

58. Grohmann CH. Evaluation of TanDEM-X DEMs on selected Brazilian sites: Comparison with SRTM, ASTER GDEM and ALOS AW3D30. Remote Sensing of Environment. 2018; 212:121–133. https://doi.org/10.1016/j.rse.2018.04.043

59. Doña C, Chang NB, Caselles V, Sánchez JM, Pérez-Planells L, Bisquert MDM, et al. Monitoring Hydrological Patterns of Temporary Lakes Using Remote Sensing and Machine Learning Models: Case Study of La Mancha Húmeda Biosphere Reserve in Central Spain. Remote Sensing. 2016; 8(8):618. https://doi.org/10.3390/rs8080618

60. Perin V, Tulbure MG, Gaines MD, Reba ML, Yaeger MA. A multi-sensor satellite imagery approach to monitor on-farm reservoirs. Remote Sensing of Environment. 2021; p. 112796. https://doi.org/10.1016/j.rse.2021.112796

61. Ferrier P, Crebassol P, Dedieu G, Hagolle O, Meygret A, Tinto F, et al. VENµS (Vegetation and environment monitoring on a new micro satellite). In: 2010 IEEE International Geoscience and Remote Sensing Symposium; 2010. p. 3736–3739.

62. Perin V, Roy S, Kington J, Harris T, Tulbure MG, Stone N, et al. Monitoring Small Water Bodies Using High Spatial and Temporal Resolution Analysis Ready Datasets. Remote Sensing. 2021; 13(24):5176. https://doi.org/10.3390/rs13245176

63. Farr TG, Rosen PA, Caro E, Crippen R, Duren R, Hensley S, et al. The Shuttle Radar Topography Mission. Reviews of Geophysics. 2007; 45(2). https://doi.org/10.1029/2005RG000183

64. Nielsen NH, Larsen MRA, Rasmussen SF. Development of a screening method to assess flood risk on Danish national roads and highway systems. Water Science and Technology. 2011; 63(12):2957–2966. https://doi.org/10.2166/wst.2011.157 PMID: 22049725

65. Boisson A, Villesseche D, Selles A, Alazard M, Chandra S, Ferrant S, et al. Long Term Monitoring of Rainwater Harvesting Tanks: Is Multi-Years Management Possible in Crystalline South Indian Aquifers? Hydrological Processes. 2022; n/a(n/a):e14759. https://doi.org/10.1002/hyp.14759

66. Ferrant S, Pascal C. Subsample of the maximum Water Area Extent of Telangana Rainwater Harvesting System from Pléiades DEM. 2023. https://doi.org/10.5281/zenodo.10402355

67. Domeneghetti A, Schumann GJP, Frasson RPM, Wei R, Pavelsky TM, Castellarin A, et al. Characterizing water surface elevation under different flow conditions for the upcoming SWOT mission. Journal of Hydrology. 2018; 561:848–861. https://doi.org/10.1016/j.jhydrol.2018.04.046